12-2006

Diel and Tidal Rhythms of Emercenge Events Based on Acousitc Observations in a Shallow Estuary

Mei Sato

DIEL AND TIDAL RHYTHMS OF EMERGENCE EVENTS BASED ON ACOUSTIC OBSERVATIONS IN A SHALLOW ESTUARY

By

Mei Sato

B.S. Tokyo University of Fisheries, 2004

A THESIS

Submitted in Partial Fulfillment of the

Requirements for the Degree of

Master of Science

(in Oceanography)

The Graduate School

The University of Maine

December, 2006

Advisory Committee:

Peter A. Jumars, Professor of Marine Sciences, Advisor

David W. Townsend, Professor of Marine Sciences

Lee Karp-Boss, Research Assistant Professor of Marine Sciences

DIEL AND TIDAL RHYTHMS OF EMERGENCE EVENTS BASED ON ACOUSTIC OBSERVATIONS IN A SHALLOW ESTUARY

By Mei Sato

Thesis Advisor: Dr. Peter A. Jumars

An Abstract of the Thesis Presented
in Partial Fulfillment of the Requirements for the
Degree of Master of Science
(in Oceanography)
December, 2006

Field observations of emergence events by epibenthic animals were conducted with two Tracor Acoustic Profiling Systems (TAPS) in the Damariscotta River estuary, Maine, in fall 2005 and summer 2006. Spectral analysis revealed that periodic temporal variability of the acoustic signals was concentrated at four periods. One was the solar day (24 h) and the other three were lunar tidal periods of 25.82 (diurnal or O_1), 12.42 (semidiurnal or M_2) and 6.21 h (half the semidiurnal period). The mysid *Neomysis americana* showed strong nocturnal migration patterns of water-column activity during its peak summer emergence season, regulated by the diel cycle. Toward the end of the emergence season in fall, however, as phytoplankton standing stocks waned, the dominant rhythm regulating their behavior shifted from a diel to semidiurnal. The timing of mysid abundance peaks in the fall coincided with low slack tides near the surface, but with maximal flood tidal speed near the bottom, providing a plausible mechanism of

retention and selective tidal stream transport within the estuary, respectively. Behaviors of smaller organisms, most likely dominated by copepods, were regulated by both M_2 and half of M_2 components. The phase difference between the acoustic backscatter and the tidal currents suggests that the signal results from smaller organisms emerging into the water column, instead of resuspension of sediment by tidal currents. The timing of their emergence varies depending on TAPS frequency, suggesting emergence by several species. Changes in the magnitudes of each frequency component in the power spectrum can be related to ontogenetic changes in behavior of mysids, intensity of tides, and seasonal food availability. This study suggests the multiple emergence events may affect the degree of benthic-pelagic coupling and reveals the mechanism of previously observed phenomenon (midnight sinking and dawn ascent) by increased sampling resolution.

Acknowledgements

This work was supported by ONR Grant N00014-03-1-0776. I thank my advisor, Peter A. Jumars, for his advice and support throughout my graduate tenure; my committee, Dr. Lee Karp-Boss and Dr. David W. Townsend, for their helpful comments; Dr. Charles Greenlaw and Dr. D. Van Holliday for their enormous support in calibrating and repairing instruments; Shawn Shellito, for his help on field observation in 2005 and precise advice and extensive knowledge about TAPS and its field deployments throughout the project; Diving officer, Chris Rigaud, for his extensive support on field observations including deployments and diving throughout the field observations in 2005 and 2006; Boat captain, Robert L. Downs, for his extensive support on field observations, especially TAPS deployment in its huge frame; Dr. Mary Jane Perry for kindly lending me her optical instruments throughout the project, advice on understanding chlorophyll variability, and providing me the PAR data; Emily Kallin, Brandon Sackman, Dave Kallin and Caleb Carter for their kind support of deploying optical instruments and calibration procedures; Brian Thompson for providing me chlorophyll, salinity and temperature data collected at the Darling Marine Center; Randy Jones for his help with field observations in summer 2006; and Kelly Dorgan for her comments and advice throughout my graduate career and for making my time in the laboratory much more enjoyable.

TABLE OF CONTENTS

LIST OF TABLES

LIST OF FIGURES

Chapter 1

INTRODUCTION

The mechanism of vertical migration is incompletely understood, and the questions as to whether some life stages and species of zooplankton and zoobenthos migrate remain unanswered. Emergence, a behavior in which nominally benthic animals swim into the water column and then return to the seabed, has been studied in terms of timing, proximate cues, ultimate causes, and abundances. Temporary emergence of benthic animals into the water column has been found in many taxa, including mysids (Takahashi and Kawaguchi 1997; Kringel et al. 2003; Abello et al. 2005; Taylor et al. 2005), copepods (Walters and Bell 1986; Thistle 2003), amphipods (DeWitt 1987), benthic ostracods and platyhelminths (Armonies 1988).

There are several hypotheses of the emergence behavior in terms of both diel and tidal cycles, which include feeding, predator avoidance, relief from low oxygen concentration, mating, horizontal transport, and retention. For emergence behavior coinciding with a diel cycle, the predominant hypothesis argues that nocturnal vertical migration enables migrants to feed on pelagic resources, such as phytoplankton and microzooplankton, which occur in higher densities near surface waters (Hays 2003). Secondly, there is extensive evidence that the ultimate function of nocturnal migration is to reduce the risk of predation from visual predators such as fish, the so-called predator evasion hypothesis (De Robertis et al. 2000; Hays 2003). Nocturnal emergence could also be a response to deteriorating conditions in the sediment. For example, at night, when photosynthesis has stopped, the zero oxygen concentration isocline in the sediment can rise to the vicinity of the sediment-water interface and stress aerobic animals (Vopel

et al. 1996, 1998), a stress that could be relieved if they move temporarily into the water column. Mating of mysids usually takes place at night (Mauchline 1980), and could be one other reason for nocturnal migration during the breeding season. Selective tidal stream transport (STST), which is a horizontal transport accomplished by synchronizing behavior with directional changes of tidal currents, has been suggested for tidally oriented migration behavior (Forward and Tankersley 2001). In coastal and estuarine areas, animals ascend from the bottom and are carried by tidal currents during one phase of the tide (ebb- or flood-tide). During slack water, at the end of this tidal phase, they return to the bottom and remain there during the opposite tidal phase. STST is a highly effective means of horizontal movement for life-history stages that have weak swimming abilities and for energy conservation by adults with strong swimming ability. Frequently, the direction of STST reverses within a species, especially at different physiological or life-cycle stages. Similarly, retention can be achieved by ascending in the water column during the times of slack water and residing near the bottom during strong ebb- and flood-tide (Wooldridge and Erasmus 1980).

The focus of this study is the mysid, *Neomysis americana*, which is the numerical and biomass dominant migrating species at the study site in the Damariscotta River estuary. In some locations, mysid swarms can reach densities of up to ~ 6×10^5 m^{-3} (Jumars 2007). Therefore, emergence can be an important component of benthic-pelagic coupling, transferring organic matter vertically between the bottom and the water column and horizontally along the whole continental margin (Marcus and Boero 1998). The organic matter comes from the animals themselves, as well as the non-living organic matter that they carry. Mysids and some other benthopelagic crustaceans (especially the

isopods *Eurydice* and decapod larvae) are the only vectors able to achieve transport of benthic matter directly up to the surface above the whole continental shelf and even the slope (Marcus and Boero 1998). Holopelagic animals can only ensure this upward transfer of benthic matter indirectly by predation of hyperbenthic organisms (Macquart-Moulin and Ribera Maycas 1995). Roast et al. (2004) documented a significant role of mysids in resuspension of sediments resulting in the turbidity maximum of an estuary. Recently conducted field measurements in Saanich Inlet, British Columbia, revealed that turbulence was increased by three to four orders of magnitude during the vertical migration of krill, with implications for nutrient mixing when waters are strongly stratified (Kunze et al. 2006).

Emergence has been studied on a variety of temporal scales, including seasonal (Pinot and Jansa 2001; Thistle 2003) and lunar (Pinot and Jansa 2001), but diel (Herman 1963; Pinot and Jansa 2001; Abello et al. 2005) and tidal (Fleeger et al. 1984; Bell et al. 1988; Taylor et al. 2005) cycles have been particular foci. Field studies treating both diel and tidal cycles at the same time are limited (e.g., Palmer 1967; Saigusa 2001), however, due to relatively short observation periods compared to the spring-neap tidal cycle. Although a number of studies suggest tidally cued vertical migration, the exact timing of migration relative to tidal cycles has not been resolved in the field due to two major limitations in previous studies: (1) vertical and (2) temporal sampling resolution. Sampling zooplankton is technically challenging. Any sampling method carries its inherent shortcomings and biases (Wiebe and Benfield 2003). Plankton nets are often towed obliquely from the bottom to the surface or at two depths, one near the bottom and one near the surface (e.g., Wooldridge and Erasmus 1980; Gagnon and Lacroix 1981;

Kimmerer et al. 1998), with imprecise control over the depths at which the net fishes. Although the development of acoustic instruments equipped with higher vertical resolution solve the problem of vertical sampling resolution, mean, median, or depth-integrated volume backscattering strength (e.g., Kringel et al. 2003) or depth-integrated total biovolume (e.g., Taylor et al. 2005) have been used to remove depth dependent trends and generate whole-water-column generalizations.

Migration patterns are expected to be depth dependent, because both of the major cues of migration, tidal currents and light, vary with depth. Estuaries have a two-layered circulation system, in which residual currents (with the tidal fluctuations removed) have net outflow in the surface layer, net inflow in the bottom layer, and a middle depth without net horizontal flow (Forward and Tankersley 2001). Low sampling frequency of a few times per tidal cycle (e.g., Wooldridge and Erasmus 1980; Palmer and Brandt 1981; Kimmerer et al. 1998) is insufficient to resolve the timing of emergence. Studies focused on light-cued emergence can be conducted in < 24 h (e.g., Teasdale et al. 2004), but in order to resolve tidal cycles, time series of ~ 2 wk are required (e.g., Saigusa 2001; Taylor et al. 2005). Even with a long record, a commonly used statistical method, autocorrelation, detects the most dominant periodicities but tends to mask weaker ones that may be present (e.g., Saigusa 2001; Abello et al. 2005; Taylor et al. 2005). In addition, the timing of emergence regulated by more than two rhythms is hard to interpret from crosscorrelograms (e.g., Taylor et al. 2005) or covariances (e.g., Kimmerer et al. 1998). Thus, previous studies tend to fail in resolving even two dominant frequencies at the same time, leading to the potential misunderstanding of some phenomena affected jointly by the combinations.

The mysid shrimp, *N. americana*, inhabits coastal and estuarine waters in depths from < 1 to 250 m along the eastern coast of North America from southern Newfoundland to northern Florida. It is important in the food web, feeding on detritus, organic-matter-covered sediments, phytobenthos, phytoplankton, smaller zooplankton (Mauchline 1980), and heterotrophic protists (David et al. 2006). In turn, it is fed upon by a wide variety of predators including cod, *Gadus morhua* (Link and Garrison 2002), Atlantic herring, *Clupea harrengus* (Hanson and Choinard 2002), weakfish, *Cynoscion regalis* (Lankford and Targett 1997), smelt, *Osmerus mordax* (Dodson et al. 1989), drum, *Larimus fasciatus* (Ross 1989), hake, *Urophycis regina* (Rachin and Warkentine 1988), bluefish, *Pomatomus saltatrix* (Friedland et al. 1988), and tomcod, *Microgadus tomdoc* (Grabe 1980).

N. americana in the northwest Atlantic produces two generations per year (Pezzack and Corey 1979). The overwintering generation matures in spring, releases their first brood within a short period, then produces a second brood (Fig. 1.1). The breeding adults die soon after producing the second brood. The first and second cohorts mature and produce a new overwintering generation and they do not survive far into winter (Mauchline 1980). Mysids carry their embryos in a marsupium within which the entire larval development takes place. Young mysids emerge from the marsupium at an early juvenile stage of development (Mauchline 1980). In the Damariscotta River estuary, *N. americana* is present weeks before any appreciable vertical migration begins (Jumars 2007). Onset of nocturnal emergence coincides with the termination of the annual alewife, *Alosa pseudoharrengus*, run upstream (Jumars 2007); emergence didn't start until late June in 2005 and mid-July in 2006. Field observations correspond to the

period of the breeding season (collected in 2006) and that of the end of the breeding season or production of the second overwintering cohort (collected in 2005).

Understanding the emergence patterns is important in order to quantify the effects of spatially and temporally varying mysid emergence on benthic-pelagic coupling. Including the depth dependent emergence rhythms and relative importance of dominant cycles will improve its quantification. Innovative, nonintrusive acoustical methods were used for field observations, with emergence traps as a direct water sampling method. In this study, spectral analysis was employed to resolve the frequencies responsible for temporal variance in the data at a few selected distances from the seabed. Then cross-spectral analysis was used to resolve phasing between emergence patterns and tidal currents. My objective was to investigate whether there is any change in dominant periodicity of emergence by mysids and smaller animals with depth and to resolve the exact timing of emergence events in relation to diel and tidal periodicities.

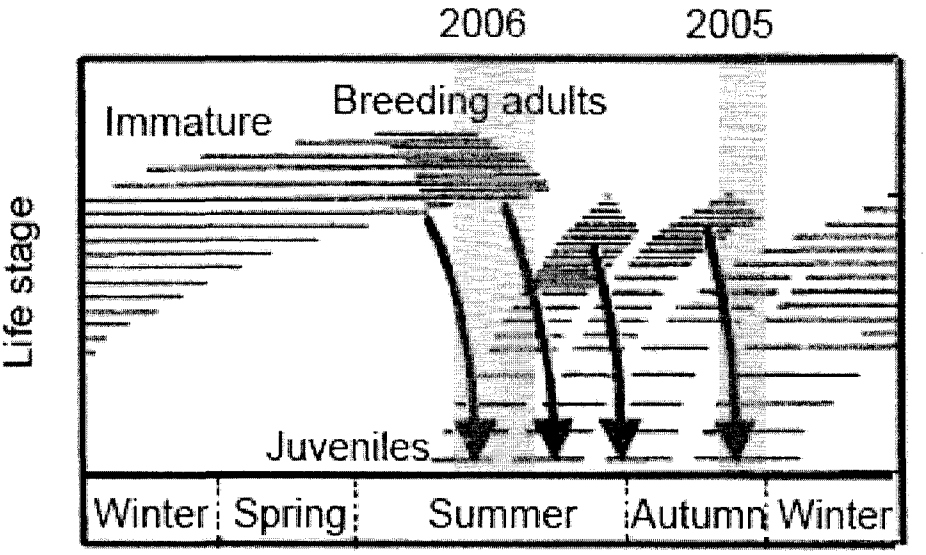

Figure 1.1. Schematic of the seasonal composition in life stages of a population of *Neomysis americana* producing two generations per year. The juveniles (sparse hatching) develop into immature adults (denser hatching), then adults (densest hatching). The arrow indicates production of the next generation by the breeding adults (modified from Mauchline 1980). Approximate field observation periods in 2005 and 2006 are indicated by shaded areas.

Chapter 2

MATERIALS AND METHODS

2.1. Study Site

2.1.1. Damariscotta River estuary

Field observations of emergence were conducted at the middle of the Damariscotta River estuary (at the Darling Marine Center; 43° 56'N, 69° 35'W), Maine, USA. The Damariscotta River estuary (Fig. 2.1), located in midcoast Maine, occupies a narrow, glacially carved, drowned river valley along the central Maine coast. It extends 29 km with a width of < 1 km and is partially mixed, having a relatively small freshwater discharge from Damariscotta Lake (1-3 m^3 s^{-1}). Its tides are semidiurnal with a mean range of approximately 3 m. Water properties, therefore, closely resemble those of nearby coastal seawater. The central reaches of the estuary are highly mixed both vertically and horizontally. The seabed is unvegetated, sandy silt or silty sand (McAlice 1993; Mayer et al. 1996). The deployment site was 10-15 m deep. At spring tides, maximum current speed exceeds 0.3 m s^{-1}.

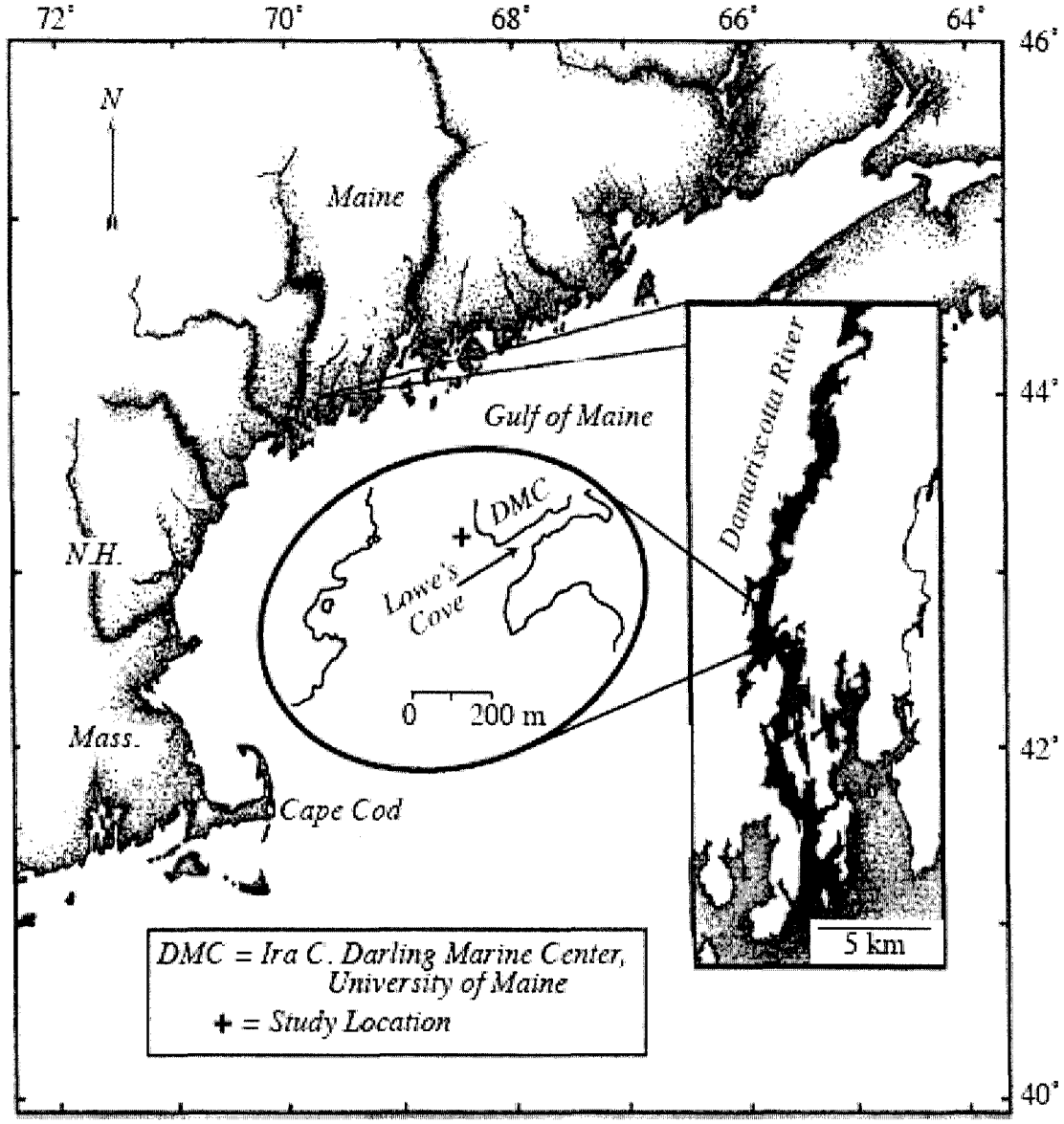

Figure 2.1. Study site in the Damariscotta River estuary, Maine.

2.1.2. Major species in the estuary

Knowledge of abundance and composition of species inhabiting in the Damariscotta River estuary is based on relatively few studies (Lee 1978; Lee and McAlice 1979; Townsend 1983; Sanders 1987; Hacunda 1989). Lee and McAlice (1979) examined the seasonal succession of *Acartia* species (*A. tonsa, A. clausi, A. longiremis*). *A. tonsa* is the most abundant species during the summer-fall period, with a density > 10^4 m^{-3}. Lee (1978) recorded cyclopoid copepds with seasonal maxima of 7,448 m^{-3} for *Hemicyclops* nauplii and 3,413 m^{-3} for *Saphirella* copepodites. Townsend (1983) identified 26 species of fish larvae from January to July collected by plankton net, with *Pholis gunnellus* numerically dominant. In terms of emergent species, *N. americana*, *Mysis mixta*, *C. septemspinosa*, cumaceans, amphipods, hydromedusae, and polychaetes were identified in emergence trap samples (Abello et al. 2005). In the Damariscotta River estuary and Jones Bay, located adjacent to the Damariscotta River estuary, crangonids, *C. septemspinosa* (Herman 1963), longhorn sculpins, *Myoxocephalus octodecemspinosus*, windowpane, *Scopthalmus aquosus*, yellowtail flounder, *Scopthalmus aquosus*, and Atlantic cod, *Gadus morhua* (Hacunda 1981) were found to be major predators of mysids.

2.2. Acoustic signatures of marine organisms

Biological sound scatterers can be divided into two groups based on differences in the acoustic signatures. One class consists of animals which contain an inclusion of gas (Fig. 2.2, a-b), such as the gas-filled swimbladder of fishes. Bubbles act as resonant scatterers. The second class of marine organisms which scatter sound includes

phytoplankton, zooplankton, and fishes without gas inclusions (Fig. 2.2, c-e). Scattering from an object which does not contain gas is largely specified by size, sound speed and density contrast with the surrounding medium, and the frequency of the sound used. Because of the wavelengths used in zooplankton acoustics, changes in the acoustic frequency can lead to either increases or decreases in scattering levels. Likewise, increases in scatterer size can lead to an increase in acoustic scattering levels, to a decrease, or to no change at all. This results from the non-monotonic character of the relationship between target strength, size, and frequency, indicating that there is no way to distinguish uniquely a change in size or a change in abundance when using a single acoustic frequency (Holliday and Pieper 1995).

Euphausiids are one of the common zooplankton groups in the world's oceans and have similar body size and large dietary breadth as mysids. The predicted maximum scattering strength for a 10 mm euphausiid is at about 240 kHz (Fig. 2.2). Thus, using theoretical approaching based on a fluid sphere model leads to the conclusion that frequencies between 50 and 500 kHz should be useful for quantitative studies of zooplankton from 5 to 40 mm in size (Holliday and Pieper 1980). Given that, *N. americana* with a body length of 6-16 mm (Mauchline 1980) should be detectable at 265-420 kHz in Tracor Acoustic Profiling Systems (TAPS). Nominal frequencies of 1100, 1850, and 3000 kHz were chosen for detecting scattering from a marine copepod about 1 mm in length, based on the scattering function predicted by the fluid sphere model, which were not harmonically related and which did not have sums or differences at any of the primary frequencies (Holliday and Pieper 1980).

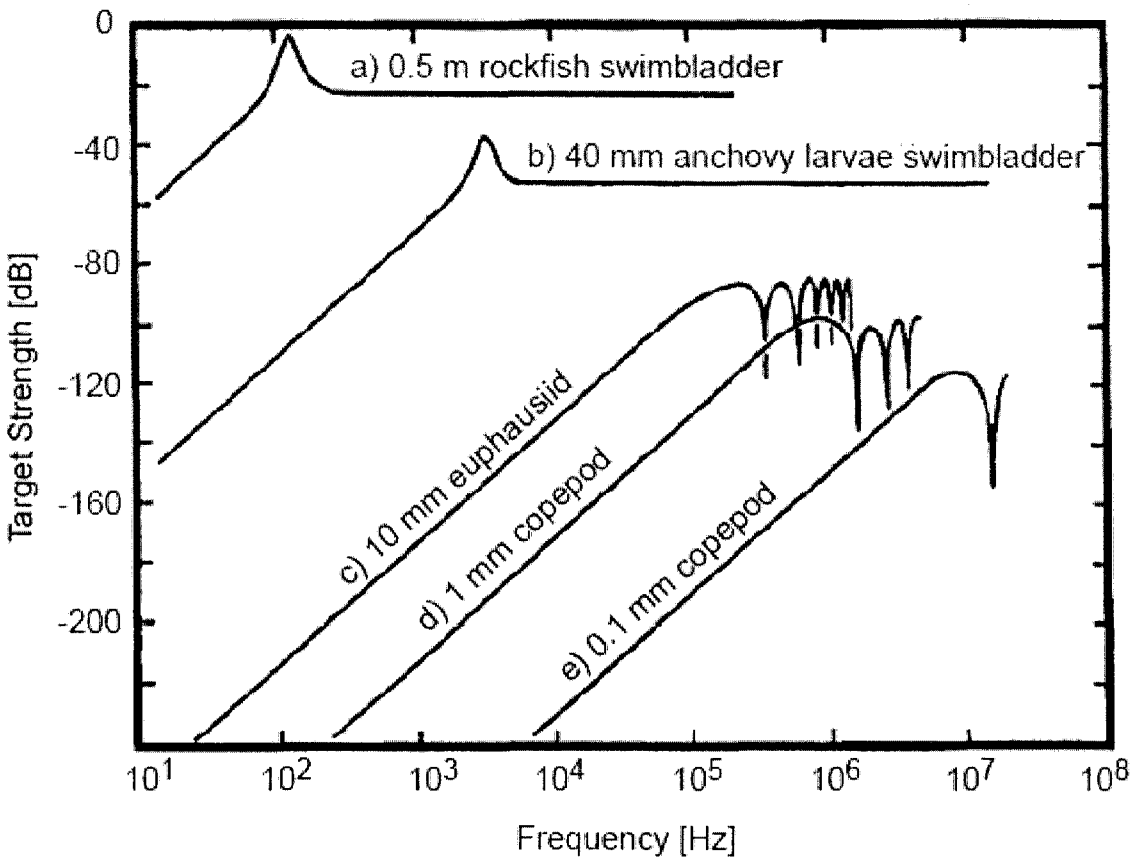

Figure 2.2. Frequency-dependent target strength (acoustic signature) of typical marine species based on theoretical models (Holliday and Pieper 1980).

2.3. Field Observations

2.3.1 Instruments

In situ acoustical sampling was conducted with two TAPS, multi-frequency echo sounders. Acoustical pulses (336 μs) were sequentially transmitted at 265, 420, 700, 1100, 1850, and 3000 kHz within a few milliseconds of each other. Echoes from particles (both biotic and abiotic) in the water column were detected at 12.5-cm intervals, and were averaged over 24 pings every minute. Because of the conical beam patterns of the transducers, sampling volumes of the bins increase with distance from the transducers. Corrections were made for spreading of the sound beam and absorption, and system calibrations were applied to convert the information to profiles of volume backscattering strength (S_v) at each frequency. Sound absorption coefficients depend on frequency, temperature, and salinity. Since the effect of salinity on sound absorption coefficients is relatively small compared to that of temperature, the mean surface salinity, measured at ~ 0.5 m depth at the dock of the Darling Marine Center and *in situ* temperature measured at the bottom of the estuary (~ 10 m in depth) were used for calculating the sound absorption coefficient. Based on the mean surface salinity and *in situ* temperature, sound speed varied from 1474-1492 m s^{-1} in fall 2005 and 1504-1510 m s^{-1} in summer 2006. Therefore, a sound wave of 265–3000 kHz had a wavelength of 0.5–5.6 mm in 2005 and 0.5-5.7 mm in 2006. Current velocities were measured by a 600-kHz Acoustic Current Doppler Profiler (ADCP) mounted on the bottom. During the observation period in 2005, a vertical bin size of 0.5 m was used, and 50 individual pings were averaged every minute. During the observation in summer 2006, a vertical bin size of 0.1 m was used, and 20 individual pings were averaged every minute. A WETLabs

BB2F combination scattering meter (470 and 700 nm) and fluorometer (ECO-BB2F) yielded chlorophyll fluorescence and also provided some indication of particle abundance. Chlorophyll fluorescence provided a crude measure of phytoplankton abundance and thus microalgal food available in the water column. The sensor was set to sample 5 times every 65 s in 2005 and a frequency of 5 min^{-1} in 2006. In 2006, the diel light regime above water at the study site was measured as photosynthetically active radiation (PAR, 400-700 nm) with a quantum sensor (LI-190SB, LI-COR Environmental, Lincoln, Nebraska) at the dock of the Darling Marine Center located close to the deployment site. A LI-1000 data logger recorded mean light intensity averaged over 10 min. All data were logged in eastern daylight savings time (EDST), stored, summarized, and analyzed with MATLAB 7.1 (Mathworks, Natick, Massachusetts). Instruments were cleaned weekly by scuba divers to control biofouling.

2.3.2. Deployment

In October through November 2005, the TAPS instruments were mounted at the bottom of the estuary as upward-looking echo sounders. Two units were placed approximately 1 mab (meters above bottom) in a metal frame, with about 50 m separation along shore. Range limitation at the higher frequencies (1850 and 3000 kHz) was caused by absorption losses in these channels. Acoustic ringing of both the metal frame and metal case of TAPS contaminated data from bins close to the TAPS transducers. The ADCP and ECO-BB2F were deployed in the proximity of the TAPS during the observation period. Given the height of the instrument (0.56 m) and the ADCP set-up

parameters, the center of the first depth cell was 2.17 mab. The ECO-BB2F, facing ~ 45° downward, was attached to the TAPS frame at 0.6 mab.

In July-August 2006, two TAPS were deployed in separate frames constructed from Schedule 30 PVC (polyvinyl chloride) plumbing pipe in an attempt to reduce ringing. One was mounted as an upward-looking echo sounder from a bottom-mounted frame. The other was operated as a downward-looking echo sounder from a 5-m tall frame (Fig. 2.3), giving significant depth overlap of all six TAPS frequencies with both TAPS units in the region near 2 mab. Spatial separation between the two TAPS along shore was 35 m. The transducer face of the upward-looking unit was placed 1 mab and that of the downward-looking unit was placed at ~ 4 mab. Acoustic ringing of the metal case or of the transducers themselves or some other near-field effect still contaminated data from bins close to the TAPS transducers. The ADCP was deployed near the TAPS with the center of the first depth cell at 1.74 mab, given the height of the instrument (0.53 m) and the ADCP set-up parameters. The ECO-BB2F was deployed on the frame of the downward-looking TAPS ~ 4 mab.

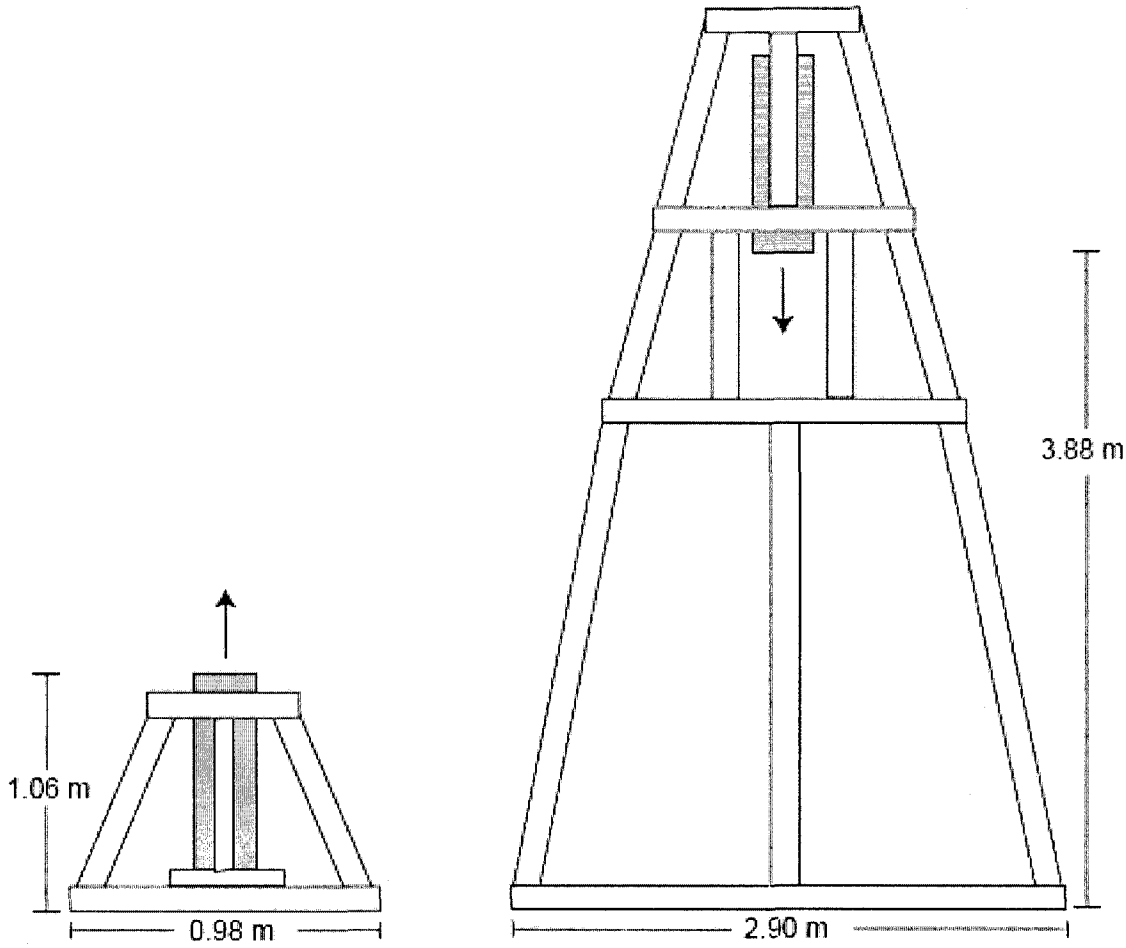

Figure 2.3. Illustration of two TAPS units (gray cylinders) in support structures made of PVC pipes. Arrows indicate directions of transducer faces.

2.3.3. Biological samples

In 2006, emergence-trap samples at the study site were collected to identify dominant migrants and their body lengths. The trap was deployed for ~ 24 h beginning in the morning on July 20, 24, 25, 26, 27, 31 and August 1, 2006. The emergence trap is pyramidal, enclosing 1 m^2 of seabed and standing 1 m high, with the faces of the pyramid covered in 1-mm Nitex netting (following Kringel et al. 2003). Specimens from traps were fixed in 10% formalin buffered with sodium tetraborate within several hours after retrieval and transferred to 70% ethanol within 3 d. Samples were sorted into taxa and counted. Total lengths (base of eyestalk to tip of telson) of *N. americana* in each sample were measured. For samples having > 250 mysids, at least 162 individuals were measured. Emergence traps alter cues, including the flow field near the bed, and may induce greater or lesser emergence than would occur in the absence of the trap, so I do not imply that trapping results are representative of emergence absent of the trap.

2.3.4. Tides

Times of predicted high and low tides at the study site (Walpole station, Maine) and 6-min predictions of tidal heights at Rockland station (44° 6.3'N, 69° 6.1'W) were obtained from NOAA (http://www.co-ops.nos.noaa.gov).

2.4. Data Analysis

Data in 2005: For chlorophyll fluorescence data, calibrations provided by WETLabs were applied to estimate chlorophyll concentration and particulate backscattering. For chlorophyll data, predicted concentrations > 2 $\mu g\ l^{-1}$ were removed and replaced by linear

interpolation, because these values were due to the temporary attachment of macroalgal fragments advected by tidal currents to the sensor face. Backscattering data coincident with the removed chlorophyll data were also removed and linearly interpolated. Since the original sampling frequency of the ECO-BB2F was 5 times $(65\ s)^{-1}$, 5 data points were averaged to have a data frequency of 1 datum $(65\ s)^{-1}$. Periods without ADCP data (maximum of 1.2 d) due to mechanical failures were linearly interpolated to form a continuous data set. Due to the different sampling frequencies among instruments (TAPS and ADCP, 1 datum min^{-1}; ECO-BB2F, 1 datum $[65\ s]^{-1}$), all data were interpolated into the lowest sampling frequency of 1 datum $(65\ s)^{-1}$ for further analysis.

Data in 2006: For the ECO-BB2F, aberrant data due to the temporary attachment of macroalgal fragments to the sensor face were again identified and removed. Then 5 data points were averaged to obtain a data frequency of 1 min^{-1}, and data gaps were filled by linear interpolation. Backscattering data corresponding to the removed fluorescence data were also removed and linearly interpolated. Fluorescence data were calibrated by measuring chlorophyll from field samples collected by Niskin bottles at ~ 4 mab, where the ECO-BB2F was deployed. Chlorophyll *a* was extracted in 90% acetone from field samples, yielding results very similar to those from application of the WETLabs calibration (Fig. 2.4). Calibrations from WETLabs were applied to particulate backscattering data. All data were interpolated into a frequency of 1 datum min^{-1} to match the sampling intervals among instruments for further analysis.

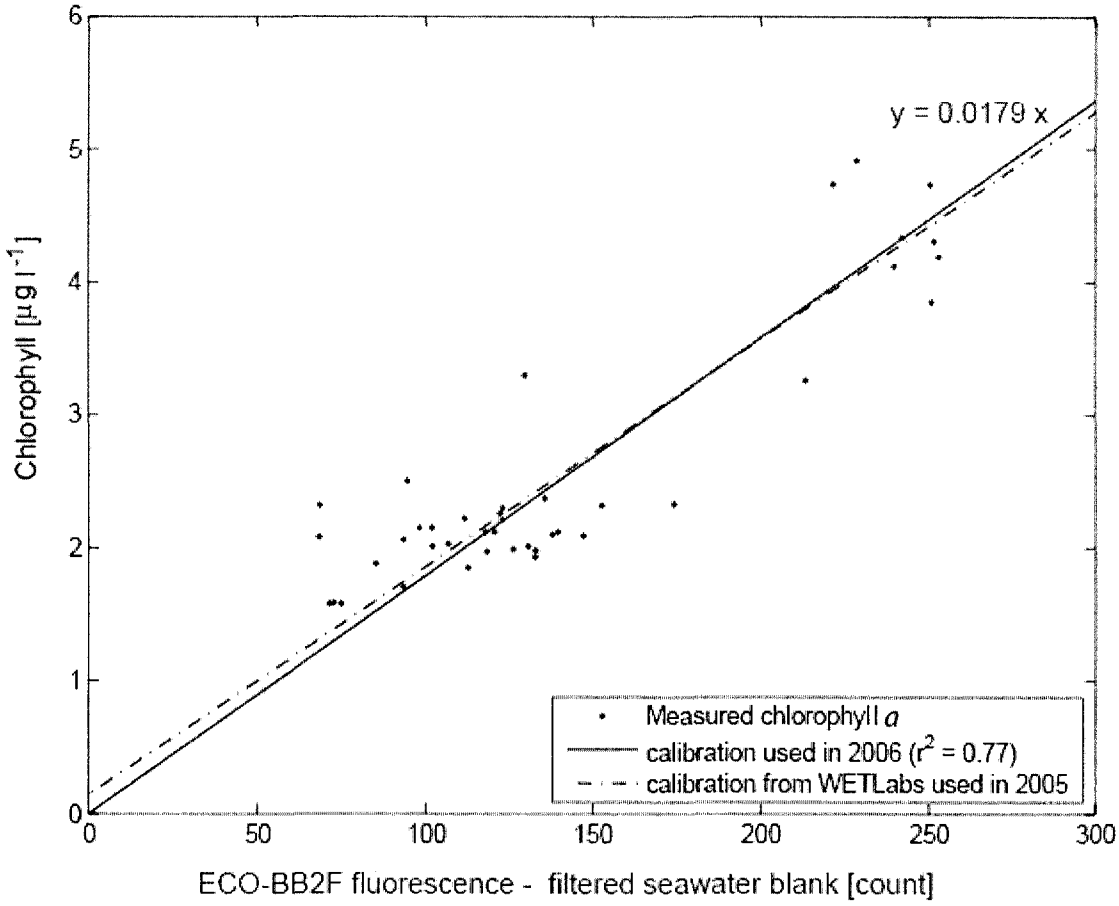

Figure 2.4. Linear regression (solid line) of fluorescence measured with an ECO-BB2F (WetLabs, Corvallis, Oregon) vs. extracted, field-collected chlorophyll *a* concentration, compared to factory calibration (dotted line).

In 2005, data collected by the two TAPS from bins at the same distance from the bottom showed similar variance, but had 2–10 dB offsets at all frequencies except 1850 kHz. Therefore, the absolute values of S_v could not be validated. In 2006, two TAPS data sets having more than 2 dB offset from each other were adjusted to match the median of the bottom-mounted TAPS. The calibration of the bottom-mounted TAPS did not change over the study period, while the calibration of the other unit was altered substantially by damage from lightning. The offsets of each TAPS data were calculated by taking 29-point median of data collected at overlapping zone during the two-week observation period. The bottom-mounted unit measured higher S_v at 265 kHz by 8 dB and at 700 kHz by 7 dB, and lower S_v at 1100 and 1850 kHz by 2 dB.

We used 7-point running medians to remove spikes apparent in the raw data and to recognize emergence patterns more clearly in echograms (Figs. 3.5-3.10 a; 3.12-3.17 a) and time-series waterfall plots (Figs. 3.4-3.12 b). For power spectral density estimates and cross-spectral analysis, means and low-frequency trends were removed from linearly interpolated data by subtracting a 2,659-point running mean in the 2005 data and a 2,881-point running mean in the 2006 data; both data lengths correspond to ~ 2 d. S_v collected at 7 and 3 mab were chosen for further analysis in 2005 in order to avoid high backscatter from surface waves and contamination from ringing of the TAPS metal frame and case. In 2006, S_v collected at 7, 3, 1 and 0.25 mab were chosen for detailed analysis.

In 2005, data collected from 16 October to 22 November 2005 were used for power spectra and cross-spectral analysis between TAPS and ADCP data, and data collected

from 14 October to 20 November 2005 were used for power spectra and cross-spectral analysis between ECO-BB2F and ADCP data. This allows the spectral analysis of each data set for the same data length, even though the data sets used in the analysis are off by 2 d.

Power spectra

Power spectra, which show the amount of variation in the data for each frequency, were estimated for all variables. After subtraction of a linear trend from the data, a Fast Fourier transform (FFT) was used to estimate spectra. In the figures I always present the range 0–5 cpd (cycles per day). As my interest is in periods of diel (24 h) light regimes and semi-diurnal tidal constituents (12.42 h), I did not consider the part of the spectrum above 5 cpd. Diel (24-h) and diurnal (25.8-h) periodicities can be resolved by the power spectral analysis for the entire observation period in 2005 (57,141 time points). The spectrum was smoothed by block averaging in order to improve statistical reliability. Block averaging of 5 segments was used in data collected in 2005. About 37 d of data (49,150 time points) were divided into subsets of 16,384 ($= 2^{14}$) points with 50% overlap. If data length was insufficient, the subset was padded with zeros to make a data segment 16,384 points long. Block averaging of 3 segments was used for the data collected in 2006. About 11 d of data (16,324 time points) were divided into subsets of 8,192 ($= 2^{13}$) data with 50% overlap. For the last subset, the subset was padded with 63 zeros to fill the data segment. This procedure produced 10 degrees of freedom in 2005 and 6 degrees of freedom in 2006 in the estimates.

Cross-spectra

Cross-spectra were calculated between variables measured by TAPS or ECO-BB2F and ADCP. B was used for variables of tidal current speeds measured by both TAPS and ECO-BB2F, and u was used for variables measure by ADCP at 3 mab in 2005 and 1.74 mab in 2006. These variables were transformed into $X_B(f)$ and $X_u(f)$ using a FFT, where f is the frequency. One-sided power spectral density of B and u are $G_{BB}(f) = 2/N\Delta t\ |X_B(f)|^2$ and $G_{uu}(f) = 2/N\Delta t\ |X_u(f)|^2$, respectively, where N is the data length and Δt is the sampling interval. The cross-spectrum of u against B is defined as $G_{uB}(f) = 2/N\Delta t\ [X_u^*(f)X_B(f)]$, where the asterisk denotes the complex conjugate, and can also be defined as $G_{uB}(f) = C_{uB}(f) - iQ_{uB}(f)$, where C is the coincident and Q is the quadrature spectrum.

The significance of the correlation is given by the coherence function γ^2 defined as

$$\gamma^2_{uB}(f) = |G_{uB}(f)|^2 / (G_{uu}(f)\ G_{BB}(f)).$$

The coherence spectrum $\gamma^2(f)$, having values between 0 and 1, is a measure of the correlation between the variations in two signals at the frequency, f.

The phase spectrum is defined as

$$\phi_{uB}(f) = \tan^{-1}[-Q_{uB}(f)/C_{uB}(f)],$$

indicating the phase difference (lead or lag) between the signals at each frequency, f. All phase spectra I present have been scaled in the region -180° to +180°. In the figures a negative value of $\phi(f)$ implies the variations of u to lead the variations of B at this frequency; for a positive phase the reverse holds. If the coherence is low for a certain frequency (i.e., not statistically significant), the phase at this frequency cannot be

estimated reliably.

The 95% confidence level for the squared coherence is

$$\gamma^2_{95} = 1 - (0.05)^{0.25} = 0.53,$$

where degrees of freedom = 10 in the 2005 data, and

$$\gamma^2_{95} = 1 - (0.05)^{0.5} = 0.78,$$

where degrees of freedom = 6 in the 2006 data (Emery and Thomson 2001).

I experimented with both the alongshore component of velocity and with speed as variables from the ADCP data for cross-spectral analysis. They showed remarkably little difference in spectra at frequencies ~ 2 cpd. In order to allow plotting of spectral power at all the frequencies of interest, I thus settled on the tidal speed at the height of interest as the ADCP variable to use in subsequent analyses and presentations.

Chapter 3

RESULTS

3.1. Abiotic and biotic parameters at the study site

3.1.1. Environmental conditions

The field observation period in 2005 corresponds to the transition from warmer to colder temperatures and low chlorophyll *a* concentration (Fig. 3.1 a). During the observation period in 2005, salinity varied from 25.6 psu to 32 psu with a mean surface salinity of 28.2 psu. Bottom-water temperature decreased from approximately 13°C at the beginning of the observation period to 8°C at the end, with maximal daily fluctuations of about 1°C due to tides (Fig. 3.1b). Chlorophyll *a* concentration was relatively constant, spanning 0.2-1 $\mu g\ l^{-1}$, with daily fluctuations due to tides (Fig. 3.1 b).

The field observation period in 2006 corresponds to warmer seasonal temperatures and relatively high chlorophyll *a* concentrations (Fig. 3.1 a). From 5 July to 4 August 2006, the salinity ranged from 26 psu to 32 psu with a mean surface salinity of 30.3 psu. From 20 July to 2 August 2006, the bottom-water temperature ranged from 15°C to 19°C with daily fluctuation of 2-2.5°C due to tides (Fig. 3.1 c). Chlorophyll *a* concentrations spanned 1-5 $\mu g\ l^{-1}$, with daily fluctuations due to tides (Fig. 3.1 c). The onset of darkness above the water, defined as < 1 $\mu mol\ quanta\ s^{-1}\ m^{-2}$, occurred between 2000 and 2040 hours and lasted until 0500 to 0520 hours. The average of daily maximum intensity of the incident PAR from 20 July to 2 August 2006 was 1525 ± 219 $\mu mol\ quanta\ s^{-1}\ m^{-2}$ (Fig. 3.1 c).

Figure 3.1. Time series of temperature, chlorophyll *a* concentration, predicted daily fluctuations in tidal level, and surface PAR at the study site (a) Time series of temperature and extracted chlorophyll *a* concentration measured at ~ 0.5 m depth at the dock of the Darling Marine Center (modified from Thompson 2006). Approximate field observation periods in 2005 and 2006 are indicated by shaded areas. Note that temperature data from 2005 were also used to show the expected monthly temperature change in 2006. (b) Predicted daily fluctuations in tidal level at the study site referenced to mean lower low water based on tide tables published by NOAA (http://www.co-ops.nos.noaa.gov), daily fluctuations of bottom-water temperature (29-point median smoothed) and chlorophyll *a* concentration (29-point median smoothed) measured at 0.6 mab (meters above bottom) in 2005. (c) Predicted daily fluctuations in tidal level at the study site referenced to mean lower low water based on tide tables published by NOAA (http://www.co-ops.nos.noaa.gov), daily fluctuations of bottom-water temperature (29-point median smoothed), chlorophyll *a* concentration (29-point median smoothed) measured at 4 mab, and surface PAR in 2006. Moon phases: (●), new moon; (○), full moon; (◖), first quarter; (◗), last quarter.

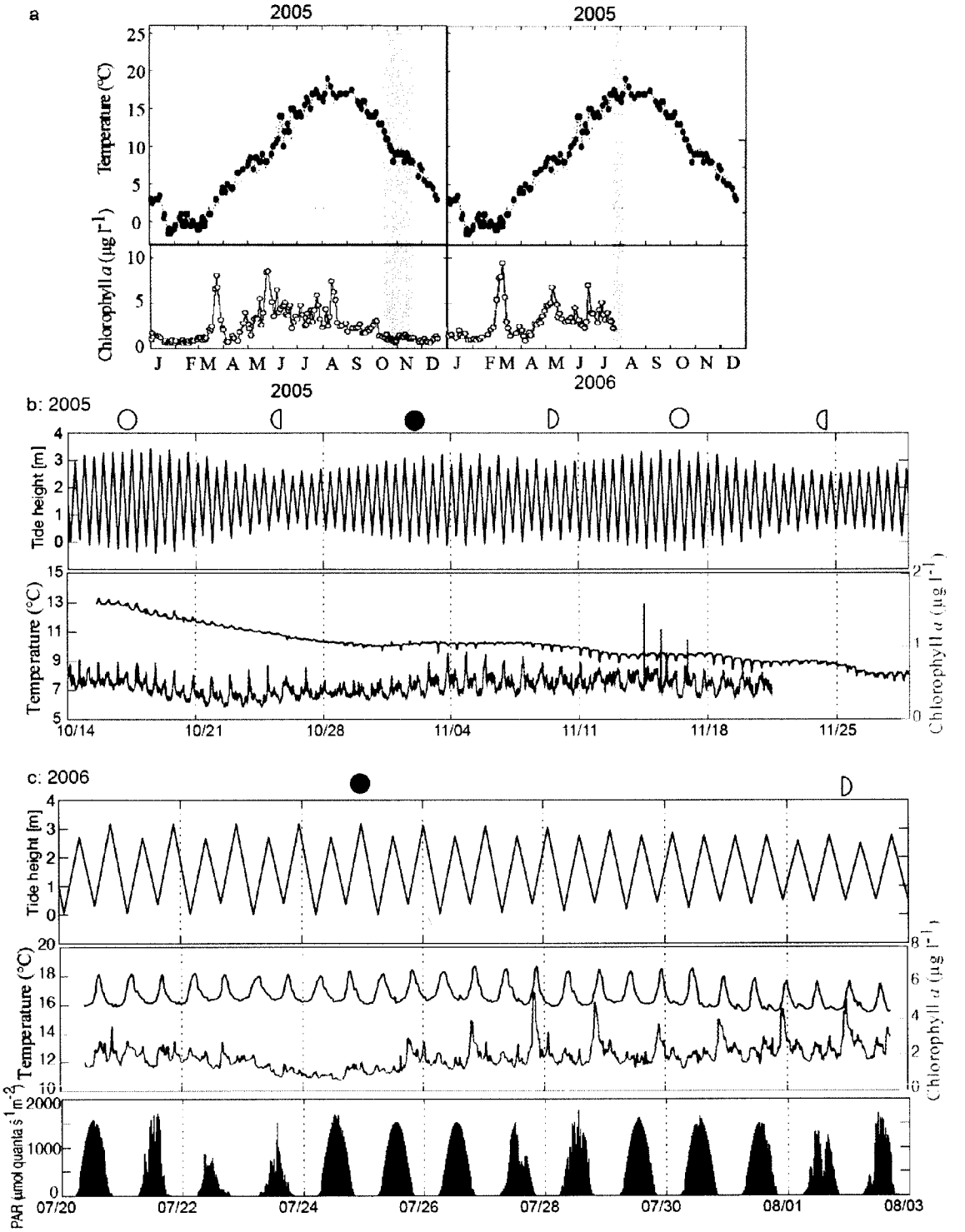
a
2005
2005
Temperature (°C)
Chlorophyll a (µg l-1)
J FM A M J J A S O N D J FM A M J J A S O N D
2005
2006
b: 2005
Tide height [m]
Temperature (°C)
Chlorophyll a (µg l-1)
10/14
10/21
10/28
11/04
11/11
11/18
11/25
c: 2006
Tide height [m]
Temperature (°C)
Chlorophyll a (µg l-1)
PAR µmol quanta s-1 m-2
07/20
07/22
07/24
07/26
07/28
07/30
08/01
08/03

3.1.2. Tidal pattern

The tidal pattern at the study site is M_2, which is the principal lunar semidiurnal constituent with a period of 12.42 h (Fig. 3.1 b, c). During spring tides, water depths at the study site were approximately 14–14.5 m depth at high tide and 9–10.5 m depth at low tide. During neap tides, the water level was approximately 13–13.5 m deep at high tide and 10.5-11 m deep at low tide. Gravitational circulation takes the form of two–layer exchange flow at the study site, which is a mean pattern of upstream bottom flow and downstream surface flow (Fig. 3.2 a1, a2). The level of no motion, the height at which this mean exchange flow equals zero, varied with tidal cycles, but is located at ~ 5 mab across the average of spring-neap cycles. Current speeds show two major spectral peaks near 2 and 4 cpd, with higher amplitude at 4 cpd (Fig. 3.2 b1, b2). Flood tides are stronger than ebb tides near bottom (Fig. 3.2 c) due to the deepening of the estuary seaward (McAlice 1993). Therefore, the spectral peak of current speeds near 2 cpd corresponds to the pattern of flood tides.

Figure 3.2. Tidal patterns at the study site based on ADCP data. (a) Tidal mean velocities at the study site based on 14-d period of ADCP data from 17 to 30 October 2005 (a1) and 11 to 24 July 2006 (a2). (b) Power spectral density (PSD) estimates of tidal current speeds at 3 mab in 2005 (b1) and at 1.74 mab in 2006 (b2). (c) Representative time series of predicted daily fluctuations in tidal level at Rockland station (44° 6.3'N, 69° 6.1'W) referenced to mean lower low water published by NOAA (http://www.co-ops.nos.noaa.gov) (c1), current speeds (c2), current velocity of North-South directions (c3), and current velocity of East-West directions (c4) at 1.74 mab at the study site. Positive values indicate northward direction (c3) and eastward direction (c4).

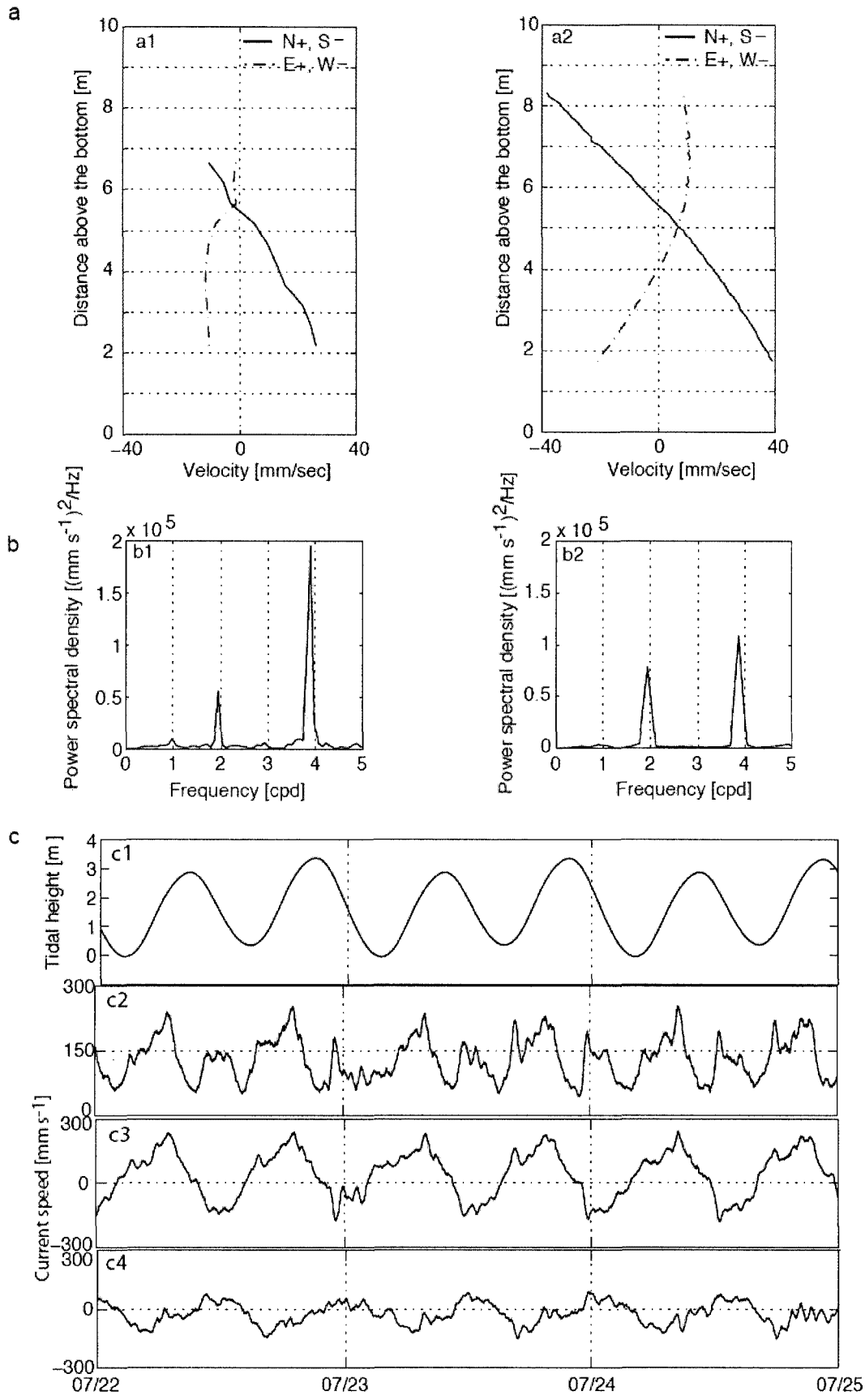
a
a1
N+, S−
E+, W−
Distance above the bottom [m]
Velocity [mm/sec]
a2
b
b1
b2
x 10^5
Power spectral density [(mm s^-1)^2/Hz]
Frequency [cpd]
c
c1
c2
c3
c4
Tidal height [m]
Current speed [mm s^-1]
07/22
07/23
07/24
07/25

3.2. Species composition at the study site and size distribution of *Neomysis americana*

N. americana, *C. septemspinosa* and *Cumacea* sp. were caught in the trap, with *N. americana* dominant, constituting more than 89% of individuals sampled (Fig. 3.3 a). A few *C. septemspinosa* were present in the samples consistently. Since they are primary predators of mysids, the presence of even one *C. septemspinosa* likely decreased the number of mysids counted in the trap. Numbers of mysids caught in the emergence trap were highest on the night of 20-21 July 2006 and lowest at the night of 26-27 July 2006, correlating inversely with the number of *C. septemspinosa* caught in the trap (Fig. 3.3 b). Average body lengths of mysids varied from 5-8 mm (Fig. 3.3 c).

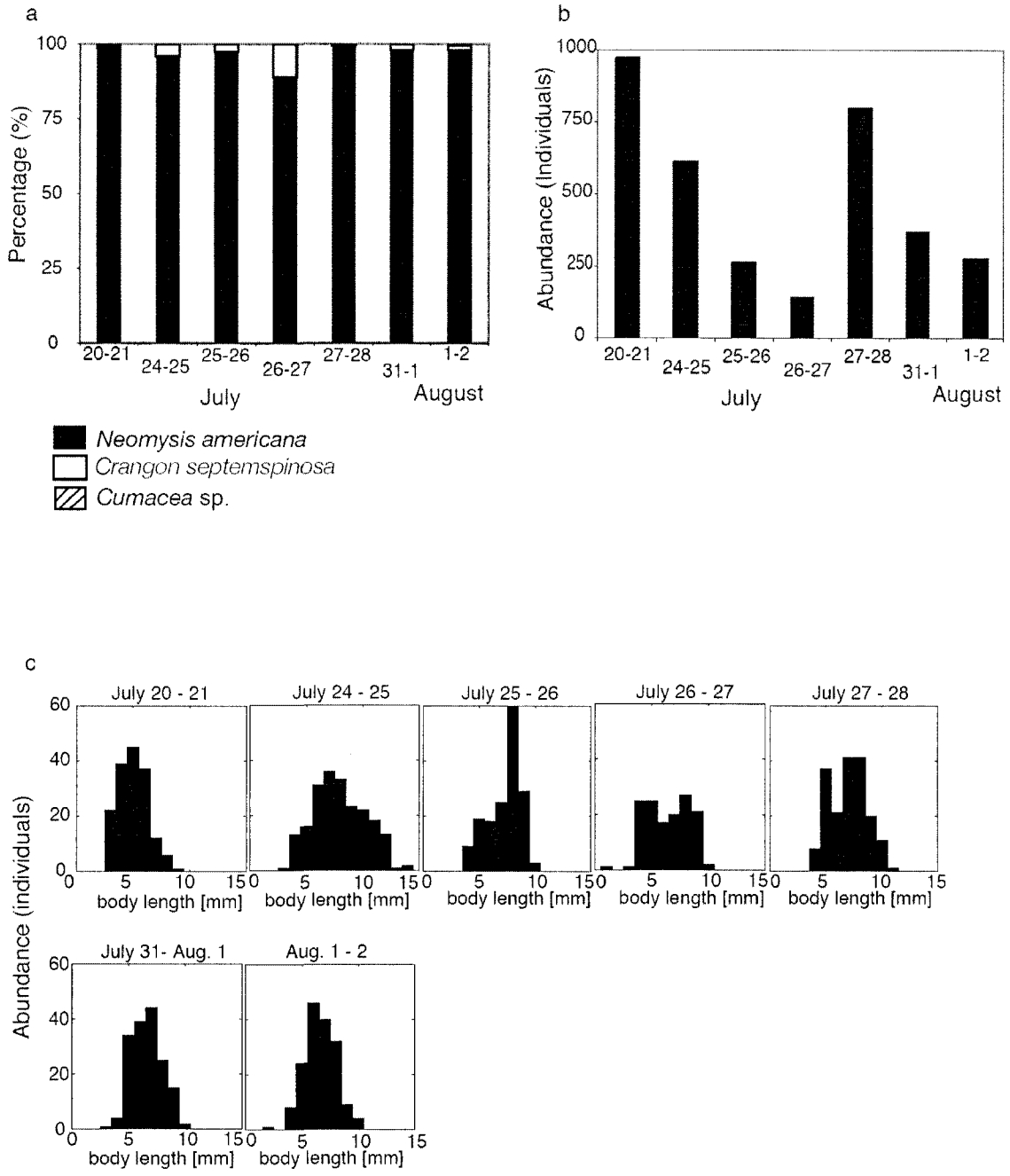

Figure 3.3. (a) Species composition in emergence-trap collections from 2006. (b) Total number of *Neomysis americana* caught in emergence traps in 2006. (c) Body lengths of the captured *N. americana*.

3.3. Emergence patterns

There are four major periods in the spectra of zooplankton, phytoplankton and suspended particles observed by acoustic and optical instruments: 24, 25.82, 12.42 and 6.21 h. A 24-h period is a diel rhythm linked to sunlight. A 25.82-h period is a diurnal or O_1 tidal constituent. Due to the limited length of field observations, the O_1 period was resolved from a diel period only in power spectrum of 2005 data. Because the block averaging for cross-spectral analysis masks the difference between a diel and O_1 periodicities, thus, phase difference of an O_1 between S_v and tides could not be determined. A 12.42-h period is an M_2 tidal constituent, which is a dominant tidal component in the study site. A 6.21-h period is half of an M_2 tidal constituent, suggesting a response to current speed (high at both mid flood and mid ebb) rather than velocity. Patterns of acoustic backscatter were examined by three approaches: echograms, time-series waterfall plots, and power spectra. The extent of the vertical migration varied with season.

3.3.1. Field observations in 2005

3.3.1.1. Rhythms involved in the observed patterns

At 265-420 kHz (Figs. 3.5-3.6 a), there was relatively high S_v throughout the water column twice a day and another S_v event occurred only in the lower water column. At 700-3000 kHz (Figs. 3.7-3.10 a), emergence events occurred twice a day throughout the water column with several additional S_v events in part of the water column over relatively short time scales.

Clear patterns of high chlorophyll *a*, particulate backscattering, and S_v at both 7 and 3 mab at all frequencies associated with tides were observed in the time-series waterfall plots. Relatively weak two diagonal trends were observed in chlorophyll *a* (Fig. 3.4 a1). In particulate backscattering data, clear patterns of two diagonal trends were observed with higher values on 15 to 21 October 2005, corresponding to new moon phase (Fig. 3.4 a2, a3). High S_v at night was observed at 7 mab during 15–26 October 2005 at 265-420 kHz (Figs. 3.5-3.6 b1). Two diagonal backscatter trends were observed at both depths at 265-420 kHz (Figs. 3.5-3.6 b1, b2) and at 7 mab at 700-1100 kHz (Figs. 3.7-3.8 b1), and four diagonal bands were observed at 3 mab at 700-3000 kHz (Figs. 3.7-3.8 b2; 3.9-3.10 b), indicating tidally correlated migration patterns. Although the time series was not long enough to resolve the long-term trend in spectral analysis, there is an indication of a lunar (spring-neap) cycle at 700-3000 kHz (Figs. 3.7-3.8 b1, b2; 3.9-3.10 b). Very low S_v occurred around 25 October and 24 November corresponding to last quarter of the moon, when the tidal range became the smallest in the lunar period of ~ 28 d.

Generally, spectral density peaks after block averaging appeared at three frequencies of 0.97, 1.95 and 3.89 cpd, which correspond to periods of 24.74, 12.31, and 6.17 h, respectively. The 24.74- and 12.31-h components were dominant in chlorophyll *a* (Fig. 3.4 b1). For particulate backscattering data, the 12.31-h component was dominant (Fig. 3.4 b2-b3). The amplitudes of the peaks were rather different across TAPS frequencies and depths in the water column. At 265 kHz, the 12.31-h component was dominant at both depths, with relatively pronounced 24.74- and 6.17-h components at 7 mab (Fig. 3.5 c2, c4). At 420 kHz, the 12.31-h component was dominant at both depths, with decreased amplitude at 3 mab, probably due to some contamination from ringing

(Fig. 3.6 c2, c4). The 24.74-h component apparent at 7 mab is a diel cycle, instead of an O_1 tidal constituent (Figs. 3.5-3.6 c1). At 700-1100 kHz, the 12.31-h period component was dominant at 7 mab (Figs. 3.7-3.8 c2) and the 24.74-h component was mostly consisted of a diel cycle (Figs. 3.7-3.8 c1). At 3 mab, the 6.17-h component was dominant, followed by 12.31- and 24.74-h components (Figs. 3.7-3.8 c2, c4), where the 24.74-h component was consisted of both a diel and an O_1 tidal component. At 1850-3000 kHz, the 6.17-h component was dominant at 3 mab, followed by the 12.31- and 24.74-h components (Figs. 3.9-3.10 c2), where the 24.74-h period was comprised of larger contribution from an O_1 tidal component than a diel cycle (Figs. 3.9-3.10 c1).

3.3.1.2. Timing of emergence

Timing of (primarily mysid) emergence associated with the day-night cycle can be clearly determined from time-series waterfall plots at 265-420 kHz at 7 mab. The 24.74-h component was relatively large (Figs. 3.5-3.6 c2) due to the patterns observed on 15-26 October 2005, when higher S_v occurred after dark.

The squared coherence spectrum and the phase spectrum were calculated to determine the correlation and the phase difference between ECO-BB2F/ TAPS data and tidal current speeds measured at 3 mab (Table 3.1). The peak of chlorophyll *a* occurred at low slack tides, with some peaks correspond to both low and high slack tides (Fig. 3.4 c1, d1). The peak of particulate backscattering coefficients coincided with flood-tide (Fig. 3.4 c2-c3, d2-d3). High coherence was observed in the 12.31- and 6.17-h components at both 7 and 3 mab at all six frequencies of TAPS. At 265 kHz, S_v led flood-tide and higher S_v coincided with the time of low slack tides near the surface (Fig.

3.5 d1, e1). Near the bottom, on the other hand, higher S_v led flood-tide by only 0.9 h, suggesting close correlation with flood tides (Fig. 3.5 d2, e2). For 6.17-h component, S_v lagged tidal speed by 2.0 h at 7 mab (Fig. 3.5 d1, e1). At 420 kHz dominated by the 12.31-h component, peak of S_v at 7 mab coincides with low slack tides (Fig. 3.6 d1, e1). At 3 mab, peak of S_v led flood-tide by 1.7 h (Fig. 3.6 d2, e2). At 700-1100 kHz, peak of S_v at 7 mab led flood-tide by 3.5-3.7 h, which coincided with close to low slack tides (Figs. 3.7-3.8 d1, e1). At 3 mab, peak of S_v at 700-3000 kHz lagged the tidal speeds by 1.5-1.8 h (Figs. 3.7-3.8 d2, e2; 3.9-3.10 d, e).

Figure 3.4. Time series and spectral analysis of chlorophyll *a* and particulate backscattering coefficients at 470 and 700 nm in 2005. (a) Temporal fluctuations of chlorophyll *a* (a1), particulate backscattering coefficients at 470 nm (a2), and at 700 nm (a3) measured at 0.6 mab plotted on a 24-h time scale. Chlorophyll *a* concentrations [μg l^{-1}] and particulate backscattering coefficients [m^{-1}] are shown only for the first date (upper left corner of each panel). (b) PSD estimates for chlorophyll *a* [(μg l^{-1})^2 Hz^{-1}] (b1), particulate backscattering coefficients at 470 nm [(m^{-1})^2 Hz^{-1}] (b2), and at 700 nm [(m^{-1})^2 Hz^{-1}] (b3). (c) Squared coherence, $\gamma^2(f)$, spectra of chlorophyll *a* (c1), particulate backscattering coefficients at 470 nm (c2), and at 700 nm (c3). Line indicates 95% confidence level. The broken line represents the value of $\gamma^2(f)$ (between 0 and 1) and the dots represent $\gamma^2(f)$ at particular frequencies (1.95 and 3.89 cpd) that contain high variance determined from PSD. (d) Phase spectra of chlorophyll *a* (d1), particulate backscattering coefficients at 470 nm (d2), and at 700 nm (d3). The broken line represents estimated phase (-180° to +180°; positive if the TAPS data lead) and the dots represent the phase at particular frequencies (1.95 and 3.89 cpd) that contain high variance determined from PSD. When coherence is high ($\gamma^2(f) > 0.53$), the phase is reliably estimated. A 24-h and 12.42-h periodicities dominate the pattern of chlorophyll *a*, coincide with low slack tides at 12.42-h periodicity. A 12.42-h periodicity dominates particulate backscattering coefficients pattern, coincident with flood-tide.

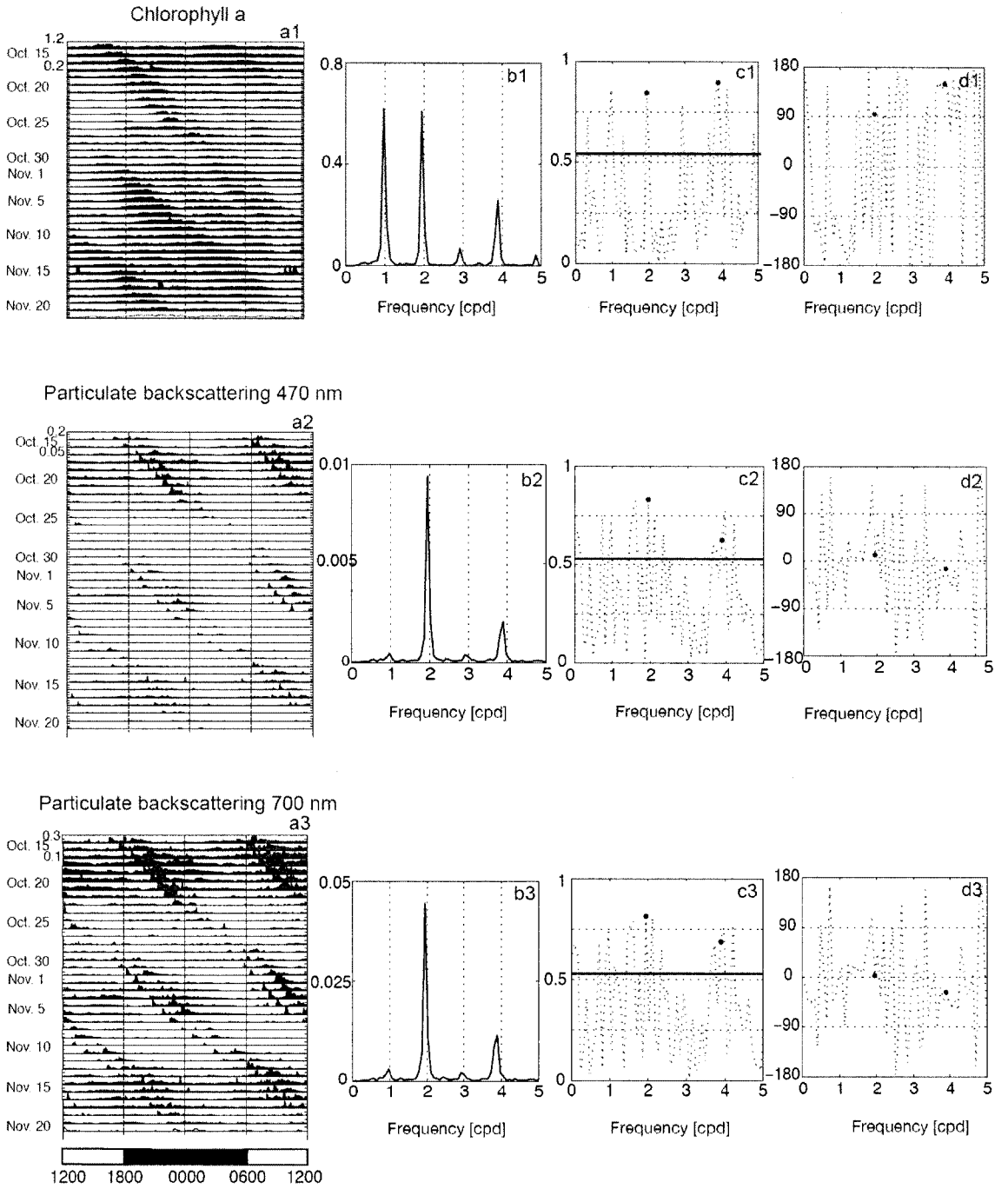
Chlorophyll a
a1
b1
c1
d1
Particulate backscattering 470 nm
a2
b2
c2
d2
Particulate backscattering 700 nm
a3
b3
c3
d3
Oct. 15
Oct. 20
Oct. 25
Oct. 30
Nov. 1
Nov. 5
Nov. 10
Nov. 15
Nov. 20
Frequency [cpd]
1200
1800
0000
0600
1200

Figure 3.5. Time series and spectral analysis of volume backscattering strength (S_v) at 265 kHz in 2005. (a) Representative echograms (265 kHz) over a 3-d period from 16 to 18 October 2005. Date tick marks correspond to midnight. Water depth varied with tidal phase, but the plot has been truncated uniformly at 10 mab. The extremely high intensities at the surface represent strong acoustic reflections from the water surface during mid to low tides. (b) Temporal fluctuations in the intensity of S_v plotted on a 24-h time scale as a waterfall plot at 7 (b1) and 3 mab (b2). Decibel levels are shown only for the first date (upper left corner of each panel). (c) Power spectral density (PSD) estimates [$dB^2\ Hz^{-1}$] for S_v using entire observation period at 7 mab (c1), block-averaged data at 7 mab (c2), entire observation period at 3 mab (c3), and block-averaged data at 3 mab (c4). (d) Squared coherence, $\gamma^2(f)$, spectra at 7 (d1) and 3 mab (d2). Line indicates 95% confidence level. The broken line represents the value of $\gamma^2(f)$ (between 0 and 1) and the dots represent $\gamma^2(f)$ at particular frequencies (1.95 and 3.89 cpd) that contain high variance determined from PSD. (e) Phase spectra [degrees] at 7 (e1) and 3 mab (e2). The broken line represents estimated phase (-180° to +180°, positive if the TAPS data lead) and the dots represent the phase at particular frequencies (1.95 and 3.89 cpd) that contain high variance determined from PSD. When coherence is high ($\gamma^2(f) > 0.53$), the phase is reliably estimated. Time series at both depths are dominated by 12.42-h periodicity (diagonal stripes in the waterfall plot) coincident with low slack tides at 7 mab and with flood-tide at 3 mab. The 7-m series shows larger contributions of diel and 6.21-h periodicities.

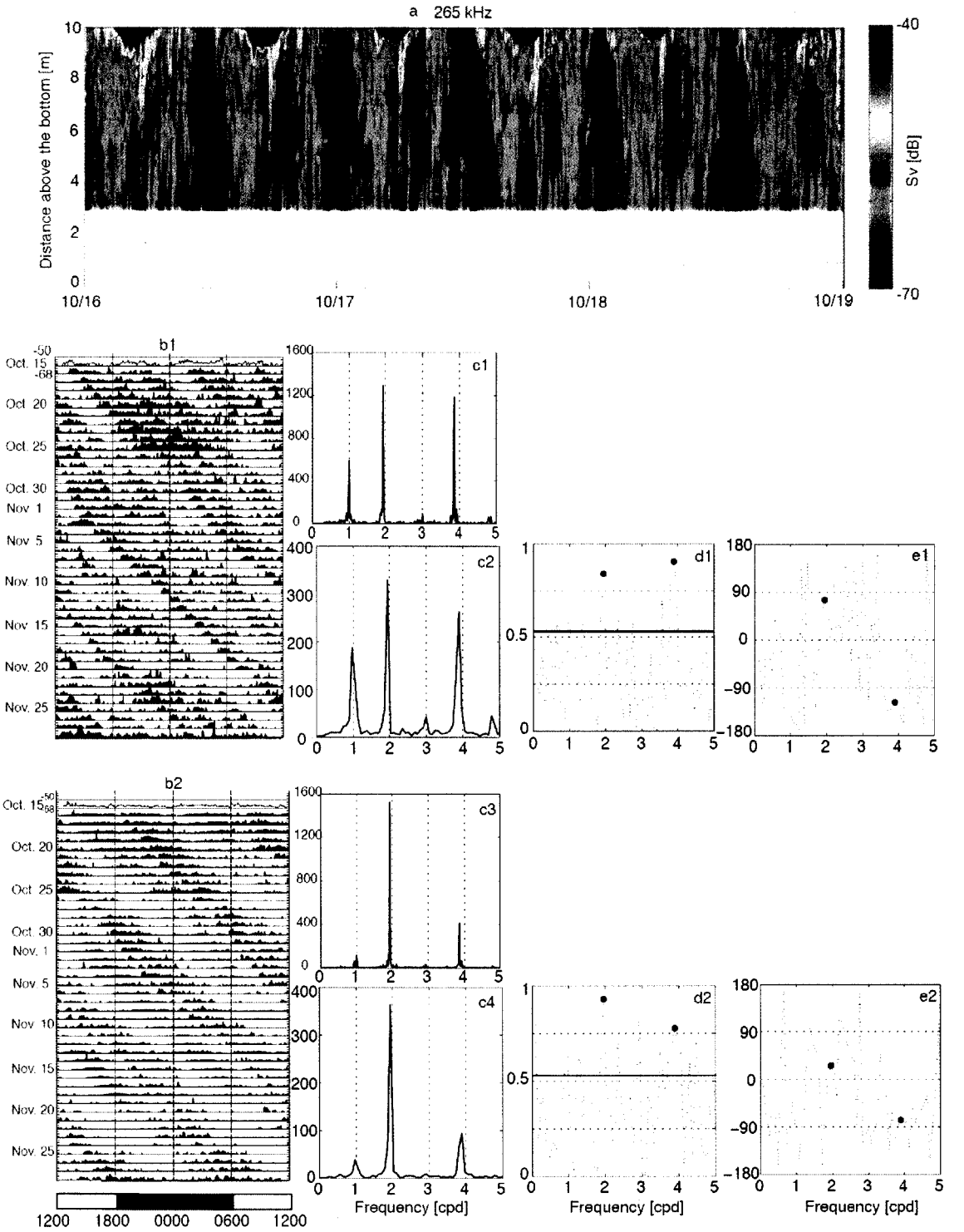
a 265 kHz
Distance above the bottom [m]
Sv [dB]
10/16
10/17
10/18
10/19
b1
b2
c1
c2
c3
c4
d1
d2
e1
e2
Oct. 15
Oct. 20
Oct. 25
Oct. 30
Nov. 1
Nov. 5
Nov. 10
Nov. 15
Nov. 20
Nov. 25
1200 1800 0000 0600 1200
Frequency [cpd]

Figure 3.6. Time series and spectral analysis of S_v at 420 kHz in 2005. (a) Representative subsets of echograms (420 kHz) over a 3-d period from 16 to 18 October 2005. Date tick marks correspond to midnight. Water depth varied with tidal phase, but the plot has been truncated uniformly at 10 mab. The extremely high intensities at the surface represent strong acoustic reflections from the water surface during mid to low tides. (b) Temporal fluctuations in the intensity of S_v plotted on a 24-h time scale as a waterfall plot at 7 (b1) and 3 mab (b2). Decibel levels are shown only for the first date (upper left corner of each panel). (c) PSD estimates [dB^2 Hz^{-1}] for S_v using entire observation period at 7 mab (c1), block-averaged data at 7 mab (c2), entire observation period at 3 mab (c3), and block-averaged data at 3 mab (c4). (d) Squared coherence, $\gamma^2(f)$, spectra at 7 (d1) and at 3 mab (d2). Line indicates 95% confidence level. The broken line represents the value of $\gamma^2(f)$ (between 0 and 1) and the dots represent $\gamma^2(f)$ at particular frequencies (1.95 and 3.89 cpd) that contain high variance as determined from PSD. (e) Phase spectra [degrees] at 7 (e1) and 3 mab (e2). The broken line represents estimated phase (-180° to +180°, positive if the TAPS data lead), and the dots represent the phase at particular frequencies (1.95 and 3.89 cpd) that contain high variance determined from PSD. When coherence is high ($\gamma^2(f) > 0.53$), the phase is reliably estimated. The 12.42-h periods dominate spectra from both depths, but the pattern at 7 mab was considerably sharper. At 12.42-h periods, S_v again led tidal velocities and with a greater phase difference at 7 mab.

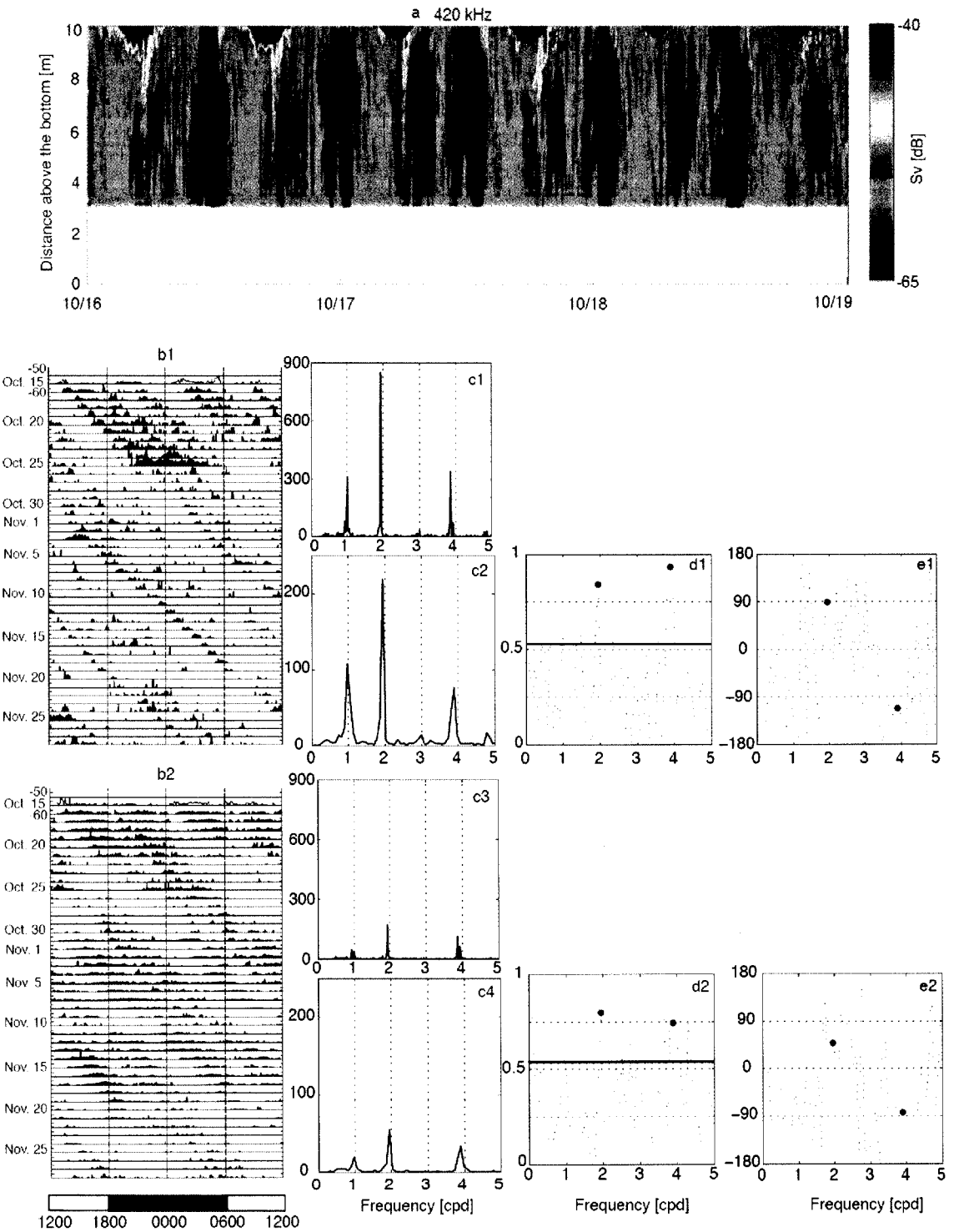
a 420 kHz
Distance above the bottom [m]
10
8
6
4
2
0
10/16
10/17
10/18
10/19
-40
-65
Sv [dB]
b1
b2
Oct. 15
Oct. 20
Oct. 25
Oct. 30
Nov. 1
Nov. 5
Nov. 10
Nov. 15
Nov. 20
Nov. 25
1200
1800
0000
0600
1200
c1
c2
c3
c4
d1
d2
e1
e2
Frequency [cpd]

Figure 3.7. Time series and spectral analysis of S_v at 700 kHz in 2005. (a) Representative echograms (700 kHz) over a 3-d period from 16 to 18 October 2005. Date tick marks correspond to midnight. Water depth varied with tidal phase, but the plot has been truncated uniformly at 10 mab. The extremely high intensities at the surface represent the strong acoustic reflections from the water surface during mid to low tides. (b) Temporal fluctuations in the intensity of S_v plotted on a 24-h time scale as a waterfall plot at 7 (b1) and 3 mab (b2). Decibel levels are shown only for the first date (upper left corner of each panel). Note that the decibel levels are chosen to show the clear pattern, therefore, it is not consistent between figures. (c) PSD estimates [$dB^2\ Hz^{-1}$] for S_v using entire observation period at 7 mab (c1), block-averaged data at 7 mab (c2), entire observation period at 3 mab (c3), and block-averaged data at 3 mab (c4). (d) Squared coherence, $\gamma^2(f)$, spectra at 7 (d1) and 3 mab (d2). Line indicates 95% confidence level. The broken line represents the value of $\gamma^2(f)$ (between 0 and 1) and the dots represent $\gamma^2(f)$ at particular frequencies (1.95 and 3.89 cpd) that contain high variance determined from PSD. (e) Phase spectra [degrees] at 7 (e1) and 3 mab (e2). The broken line represents estimated phase (-180° to +180°; positive if the TAPS data lead) and the dots represent the phase at particular frequencies (1.95 and 3.89 cpd) that contain high variance determined from PSD. When coherence is high ($\gamma^2(f) > 0.53$), the phase is reliably estimated. A 12.42-h period coincident with low slack tides dominated at 7 mab, but a larger contribution of 6.21-h periodicity lagged maximum tidal speed by 1.5 h at 3 mab.

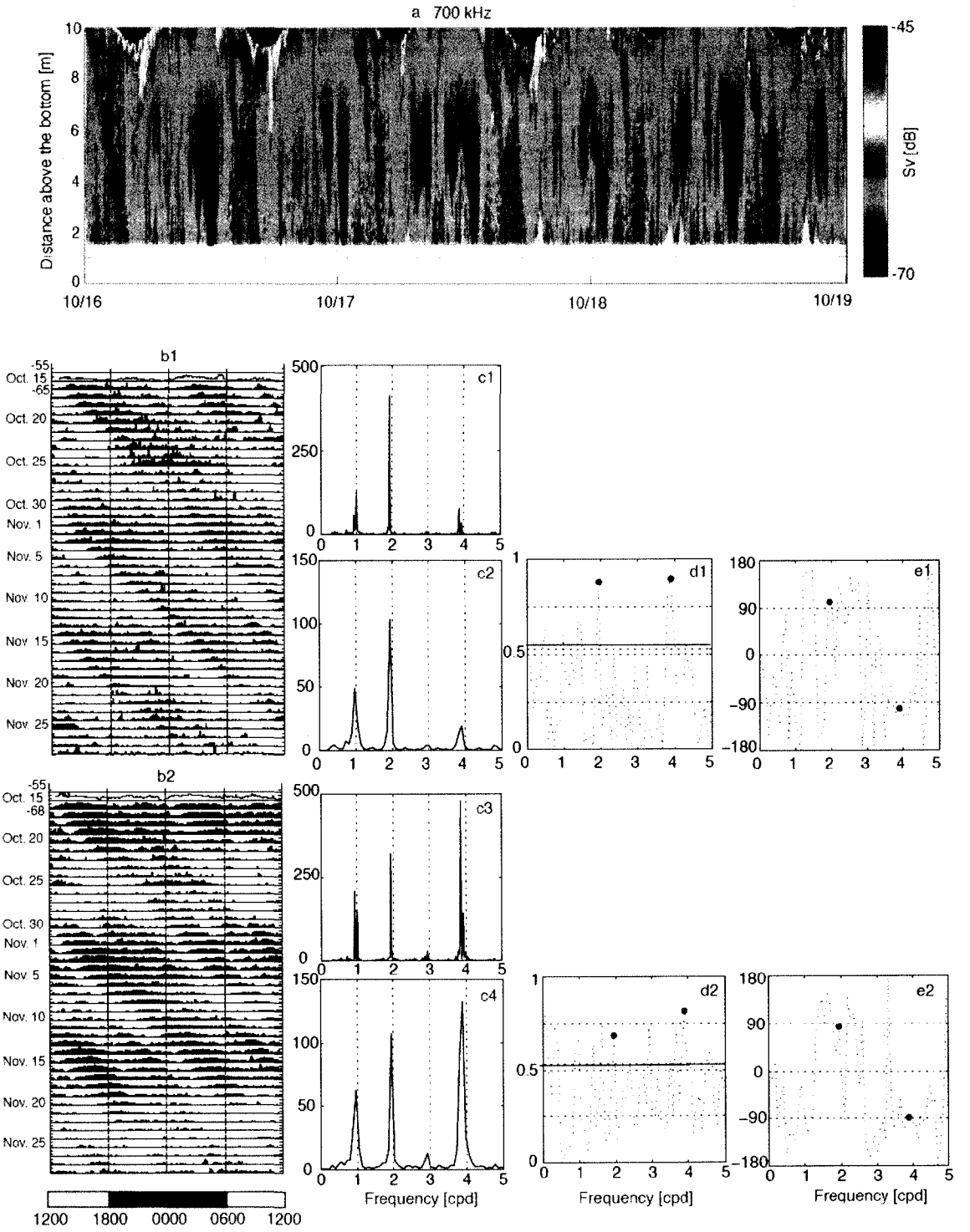
a 700 kHz
Distance above the bottom [m]
10
8
6
4
2
0
10/16
10/17
10/18
10/19
-45
-70
Sv [dB]
b1
b2
Oct. 15
Oct. 20
Oct. 25
Oct. 30
Nov. 1
Nov. 5
Nov. 10
Nov. 15
Nov. 20
Nov. 25
-55
-65
-68
1200
1800
0000
0600
1200
c1
c2
c3
c4
d1
d2
e1
e2
Frequency [cpd]

Figure 3.8. Time series and spectral analysis of S_v at 1100 kHz in 2005. (a) Representative echograms (1100 kHz) over a 3-d period from 16 to 18 October 2005. Date tick marks correspond to midnight. Water depth varied with tidal phase, but the plot has been truncated uniformly at 10 mab. The extremely high intensities at the surface represent strong acoustic reflections from the water surface during mid to low tides. (b) Temporal fluctuations in the intensity of S_v plotted on a 24-h time scale as a waterfall plot at 7 (b1) and 3 mab (b2). Decibel levels are shown only for the first date (upper left corner of each panel). (c) PSD estimates [$dB^2\ Hz^{-1}$] for S_v using entire observation period at 7 mab (c1), block-averaged data at 7 mab (c2), entire observation period at 3 mab (c3), and block-averaged data at 3 mab (c4). (d) Squared coherence, $\gamma^2(f)$, spectra at 7 (d1) and 3 mab (d2). Line indicates 95% confidence level. The broken line represents the value of $\gamma^2(f)$ (between 0 and 1) and the dots represent $\gamma^2(f)$ at particular frequencies (1.95 and 3.89 cpd) that contain high variance determined from PSD. (e) Phase spectra [degrees] at 7 (e1) and 3 mab (e2). The broken line represents estimated phase (-180° to +180°; positive if the TAPS data lead) and the dots represent the phase at particular frequencies (1.95 and 3.89 cpd) that contain high variance determined from PSD. When coherence is high ($\gamma^2(f) > 0.53$), the phase is reliably estimated. A 12.42-h tidal periodicity continued to dominate S_v at 7 mab coincident with low slack tides, as did 6.21-h periodicity lagging maximum current speed by 1.6 h at 3 mab.

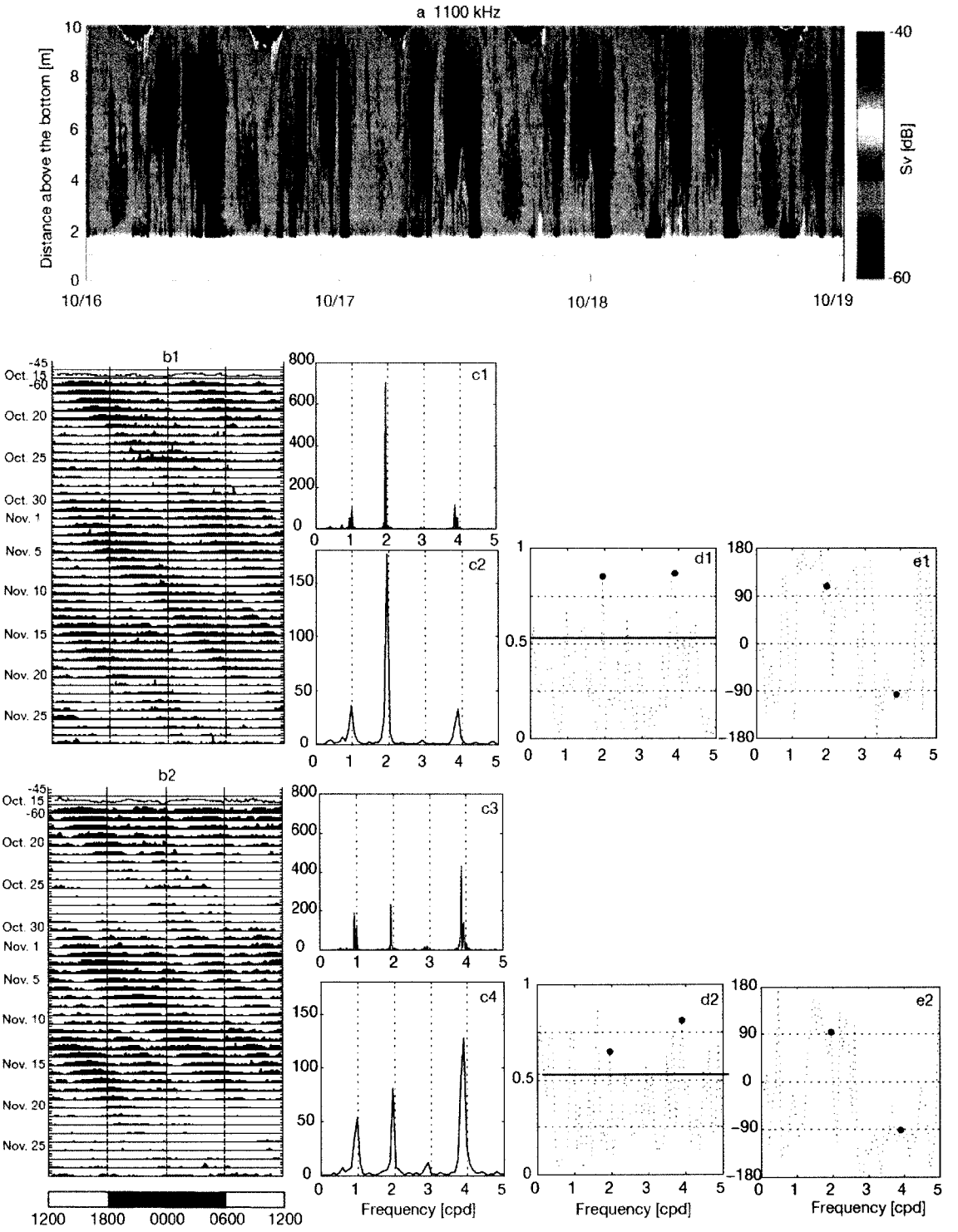
a 1100 kHz
Distance above the bottom [m]
Sv [dB]
10/16
10/17
10/18
10/19
b1
b2
c1
c2
c3
c4
d1
d2
e1
e2
Oct. 15
Oct. 20
Oct. 25
Oct. 30
Nov. 1
Nov. 5
Nov. 10
Nov. 15
Nov. 20
Nov. 25
1200
1800
0000
0600
1200
Frequency [cpd]

Figure 3.9. Time series and spectral analysis of S_v at 1850 kHz in 2005. (a) Representative echograms (1850 kHz) over a 3-d period from 16 to 18 October 2005. Date tick marks correspond to midnight. Water depth varied with tidal phase, but the plot has been truncated uniformly at 7.5 mab due to range limitation at this frequency. (b) Temporal fluctuations in the intensity of S_v plotted on a 24-h time scale as a waterfall plot at 3 mab. Decibel levels are shown only for the first date (upper left corner of each panel). (c) PSD estimates [$dB^2\ Hz^{-1}$] for S_v using entire observation period (c1) and block-averaged data (c2) at 3 mab. (d) Squared coherence, $\gamma^2(f)$, spectra at 3 mab. Line indicates 95% confidence level. The broken line represents the value of $\gamma^2(f)$ (between 0 and 1) and the dots represent $\gamma^2(f)$ at particular frequencies (1.95 and 3.89 cpd) that contain high variance determined from PSD. (e) Phase spectra [degrees] at 3 mab. The broken line represents estimated phase (-180° to +180°; positive if the TAPS data lead) and the dots represent the phase at particular frequencies (1.95 and 3.89 cpd) that contain high variance determined from PSD. When coherence is high ($\gamma^2(f) > 0.53$), the phase is reliably estimated. Range limitation prevented assessment at 7 mab, but 6.21-h tidal periodicity continued to dominate at 3 mab again lagging maximum tidal current speed by 1.7 h.

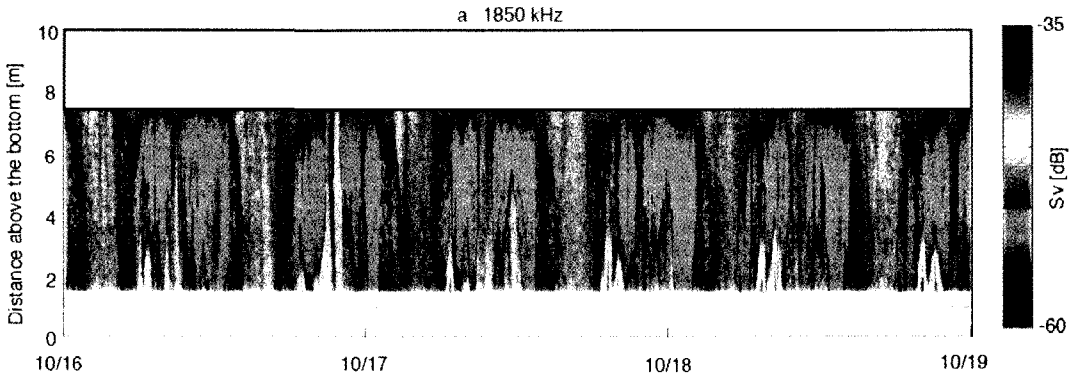
a 1850 kHz
Distance above the bottom [m]
10
8
6
4
2
0
10/16
10/17
10/18
10/19
-35
Sv [dB]
-60

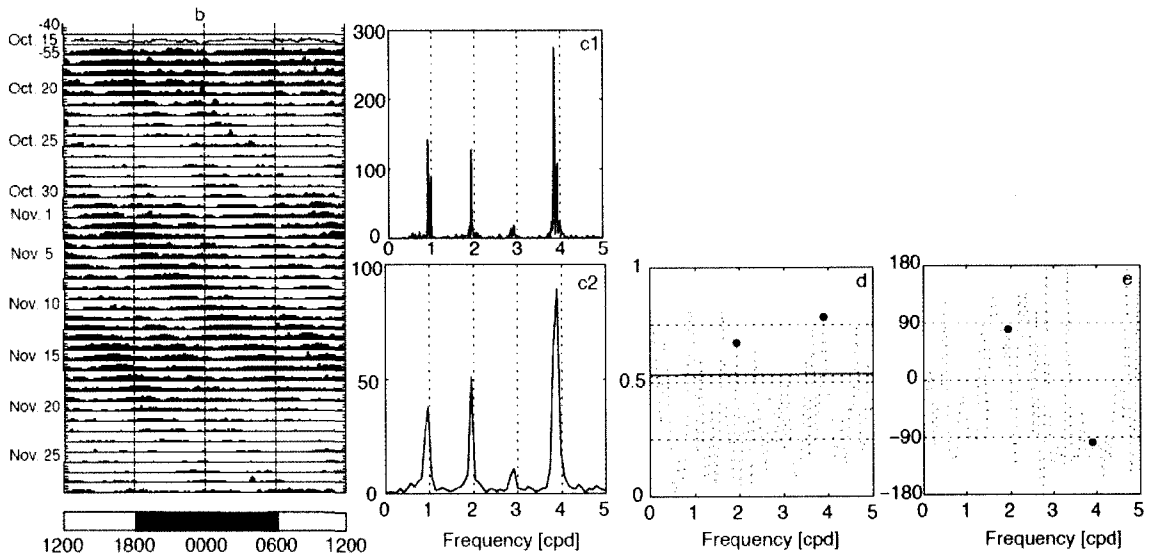
b
-40
-55
Oct. 15
Oct. 20
Oct. 25
Oct. 30
Nov. 1
Nov. 5
Nov. 10
Nov. 15
Nov. 20
Nov. 25
1200
1800
0000
0600
1200
c1
c2
Frequency [cpd]
d
Frequency [cpd]
e
Frequency [cpd]

Figure 3.10. Time series and spectral analysis of S_v at 3000 kHz in 2005. (a) Representative echograms (3000 kHz) over a 3-d period from 16 to 18 October 2005. Date tick marks correspond to midnight. Water depth varied with tidal phase, but the plot has been truncated uniformly at 5 mab due to range limitation at this frequency. (b) Temporal fluctuations in the intensity of S_v plotted on a 24-h time scale at 3 mab. Decibel levels are shown only for the first date (upper left corner of each panel). (c) PSD estimates [$dB^2\ Hz^{-1}$] for S_v using entire observation period (c1) and block-averaged data (c2) at 3 mab. (d) Squared coherence, $\gamma^2(f)$, spectra at 3 mab. Line indicates 95% confidence level. The broken line represents the value of $\gamma^2(f)$ (between 0 and 1) and the dots represent $\gamma^2(f)$ at particular frequencies (1.95 and 3.89 cpd) that contain high variance determined from PSD. (e) Phase spectra [degrees] at 3 mab. The broken line represents estimated phase (-180° to +180°; positive if the TAPS data lead) and the dots represent the phase at particular frequencies (1.95 and 3.89 cpd) that contain high variance determined from PSD. When coherence is high ($\gamma^2(f) > 0.53$), the phase is reliably estimated. Range limitation prevented assessment at 7 mab, but 6.21-h tidal periodicity continued to dominate at 3 mab again lagging maximum tidal speed by 1.8 h.

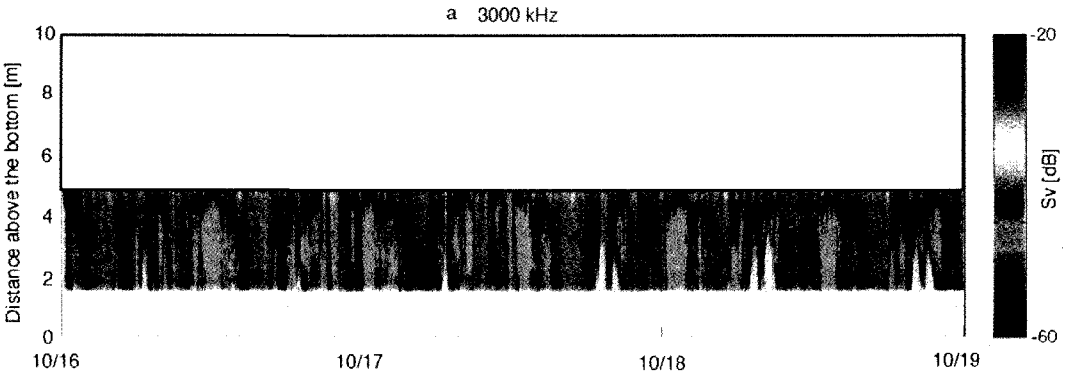
a 3000 kHz
Distance above the bottom [m]
10
8
6
4
2
0
10/16
10/17
10/18
10/19
-20
-60
Sv [dB]

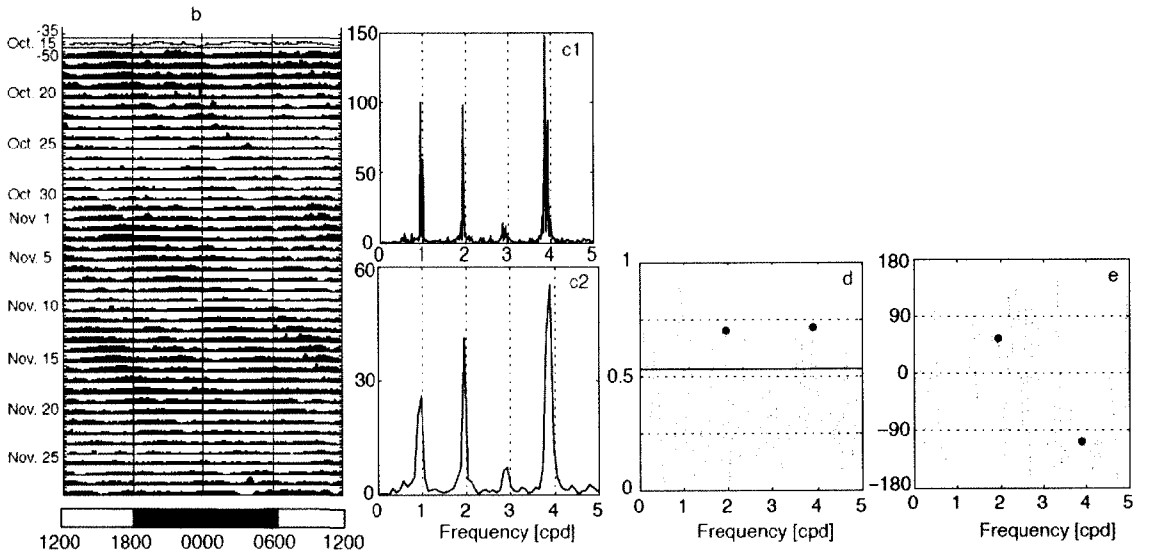
b
Oct. -35
-15
-50
Oct. 20
Oct. 25
Oct. 30
Nov. 1
Nov. 5
Nov. 10
Nov. 15
Nov. 20
Nov. 25
1200
1800
0000
0600
1200
c1
c2
Frequency [cpd]
d
Frequency [cpd]
e
Frequency [cpd]

Table 3.1. Summary of cross-spectral analyses between volume backscattering strength (S_v), chlorophyll *a*, particulate backscattering coefficients at 470 nm (bbp470), and at 700 nm (bbp700), and tidal current speeds during field observations in 2005. Statistically significant squared coherences ($\gamma^2(f) > 0.53$) are summarized. A positive value of $\phi(f)$ implies the variation of data in TAPS or ECO-BB2F data to lead the variations of ADCP data.

	Distance	M_2 cycle (12.42 h)		$M_2/2$ cycle (6.21 h)	
	[mab]	$\gamma^2(f)$	$\phi(f)$	$\gamma^2(f)$	$\phi(f)$
265 kHz	7	0.84	75° (2.6 h)	0.91	-118° (-2.0 h)
420 kHz	7	0.84	89° (3.0 h)	0.93	-112° (-1.9 h)
700 kHz	7	0.88	101° (3.5 h)	0.90	-101° (-1.7 h)
1100 kHz	7	0.85	109° (3.7 h)	0.87	-96° (-1.6 h)
265 kHz	3	0.93	26° (0.9 h)	0.78	-77° (-1.3 h)
420 kHz	3	0.80	49° (1.7 h)	0.74	-83° (-1.4 h)
700 kHz	3	0.68	84° (2.9 h)	0.82	-88° (-1.5 h)
1100 kHz	3	0.65	94° (3.2 h)	0.81	-92° (-1.6 h)
1850 kHz	3	0.67	80° (2.7 h)	0.79	-98° (-1.7 h)
3000 kHz	3	0.70	57° (1.9 h)	0.72	-107° (-1.8 h)
chlorophyll *a*	0.62	0.84	95° (3.2 h)	0.89	150° (2.6 h)
bbp470	0.62	0.83	12° (0.4 h)	0.63	-14° (-0.2 h)
bbp700	0.62	0.81	3° (0.1 h)	0.69	-27° (-0.5 h)

3.3.2. Field observations in 2006

3.3.2.1. Rhythms involved in the observed patterns

At 265-420 kHz, there was one major emergence event at night that extended throughout the water column (Figs. 3.12-3.13 a). At 700-1100 kHz, there was one major emergence event at night throughout the water column, accompanied by several small emergence events of more limited vertical extent from the bottom (Figs. 3.14-3.15 a). At 1850-3000 kHz, there were multiple emergence events throughout the day (Figs. 3.16-3.17 a).

Clear patterns of high clorophyll *a* and particualte backscatterings associated with tides were observed as two major diagonal trends (Fig. 3.11 a1-a3). At 265-420 kHz, clear patterns of high S_v at night were observed throughout the water column, with slight indications of tidal effects appearing as diagonal swaths at 3 and 1 mab at 265 kHz and significant tidal effects throughout the water column at 420 kHz (Figs. 3.12-3.13 b1-b4). High S_v continued during daylight of 21 July 2006 at 0.25 mab (Figs. 3.12-3.13 b4). At 700 kHz, patterns of high S_v associated with tides were observed throughout the water column with a clear day-night cycle at 0.25 mab (Fig. 3.14 b1-b4). At 1100 kHz, clear patterns of high S_v associated with tides were observed throughout the water column, with stronger S_v near the bottom (Fig. 3.15 b1-b4). Two diagonal swaths at 7 mab, and four diagonal swaths at 3, 1 and 0.25 mab were observed. At 1850-3000 kHz, clear patterns of high S_v associated with tides were observed throughout the water column, with stronger S_v near the bottom (Figs. 3.16-3.17 b1-b3). The tidal patterns observed at different depths were similar, in terms of two major diagonal swaths associated with two narrower (shorter-period) swaths of high backscatter.

Generally, spectral density peaks appeared at three frequencies of 1.05, 1.93 and 3.87 cpd, which correspond to periods of 22.86-, 12.44-, and 6.20-h, respectively. All these frequencies appeared as major peaks in chlorophyll *a* (Fig. 3.11 a1). For particulate backscattering data, the 12.44-h component was dominant (Fig. 3.11 a2-a3). The amplitudes of the peaks were rather different depending on TAPS frequencies and water depths. At 265-420 kHz, the 22.86-h component was dominant throughout the water column, increasing its amplitude towards the bottom (Figs. 3.12-3.13 c1-c4). Contributions of 12.44- and 6.20-h components were small or absent. At 700 kHz, both the 22.86- and 12.44-h components were strong at 7 mab (Fig. 3.14 c1), only the 12.44-h component was dominant at 3 mab (Fig. 3.14 c2), both 22.86- and 6.20-h periods were strong at 1 mab (Fig. 3.14 c3), and the 22.86-h component was dominant at 0.25 mab (Fig. 3.14 c4). At 1100 kHz, the 12.44-h component was dominant at 7 and 3 mab and the 6.20-h component became important towards the bottom (Fig. 3.15 c1-c4). At 1850 kHz, the 12.44-h component dominated throughout the water column, with equally dominant 12.44- and 6.20-h components observed at 1 mab (Fig. 3.16 c1-c3). At 3000 kHz, the 12.44-h component was dominant at 3 and 0.25 mab, but 6.20-h component was dominant at 1 mab (Fig. 3.17 c1-c3).

3.3.2.2. Timing of emergence

Chlorophyll *a* regulated by 22.86-h appeared at night (Fig. 3.11 a1). Emergence entrained to a day-night cycle can be clearly observed in the time-series waterfall plot at 265-700 kHz, whose power spectra reveal one major periodicity at

22.86-h (Figs. 3.12-3.13 b1-b4; 3.14 b4). Higher S_v occurred after dark throughout the water column.

The squared coherence spectrum and the phase spectrum were calculated to determine the correlation and the phase difference between ECO-BB2F/ TAPS data and tidal current speeds measured at 1.74 mab (Table 3.2). The peak of chlorophyll *a* led flood-tide by 1.3-h and led tidal speed by 1.9 h (Fig. 3. 11 c1, d1). The particulate backscattering coefficients led flood-tide by 2.2 h (Fig. 3.11 c2-c3, d2-d3). At 265 kHz, because peaks in 12.44- and 6.20-h components were small or absent, correlations between S_v and tidal current speeds were not significant; therefore phase differences could not be reliably estimated. At 420 kHz, variations in S_v led those in current speeds by 4.0 h at 3 mab (Fig. 3.13 d2, e2). At 700 kHz, variations in S_v led those in flood-tide by 3.4-4.2 h throughout the water column, corresponding to near low slack tides (Fig. 3.14 d1-d4, e1-e4). At 3 and 1 mab, variations in S_v at the 6.20-h period lagged those in current speeds by 1.6-2.0 h. At 1100-3000 kHz, high coherence was observed at the 12.44 and 6.20-h components throughout the water column. At 1100 kHz, variations in S_v at the 12.44-h component coincide with near low slack tides (Fig. 3.15 d1-d4, e1-e4). Over the full range of depths, variations in S_v at the 6.2-h component lagged those in current speeds by 1.5-2.0 h. At 1850 kHz, variations in S_v at the 12.44-h component corresponded to near low slack tides (Fig. 3.16 d1-d3, e1-e3). At the 6.20-h component, variations in S_v lagged those in current speeds by 1.3-2.0 h. At 3000 kHz, variations in S_v at the 12.44-h component led those in current speeds by 1.6-2.3 h (Fig. 3.17 d1-d3, e1-e3). Variation in S_v at the 6.20-h component lagged those in current speeds by 1.1-2.2 h. The phase differences decreased at both 12.44 and 6.20-h components near the bottom.

Figure 3.11. Time series and spectral analysis of chlorophyll *a* and particulate backscattering coefficients at 470 and 700 nm in 2006. (a) Temporal fluctuations of chlorophyll *a* (a1), particulate backscattering coefficients at 470 nm (a2), and at 700 nm (a3) measured at 4 mab plotted on a 24-h time scale. Chlorophyll *a* concentrations [$\mu g\ l^{-1}$] and particulate backscattering coefficients [m^{-1}] are shown only for the first date (upper left corner of each panel). (b) PSD estimates for chlorophyll *a* [$(\mu g\ l^{-1})^2\ Hz^{-1}$] (b1), particulate backscattering coefficients at 470 nm [$(m^{-1})^2\ Hz^{-1}$] (b2), and at 700 nm [$(m^{-1})^2\ Hz^{-1}$] (b3). (c) Squared coherence, $\gamma^2(f)$, spectra of chlorophyll *a* (c1), particulate backscattering coefficients at 470 nm (c2), and at 700 nm (c3) at 4 mab. Line indicates 95% confidence level. The broken line represents the value of $\gamma^2(f)$ (between 0 and 1) and the dots represent $\gamma^2(f)$ at particular frequencies (1.95 and 3.89 cpd) that contain high variance determined from PSD. (d) Phase spectra of chlorophyll *a* (d1), particulate backscattering coefficients at 470 nm (d2), and at 700 nm (d3). The broken line represents estimated phase (-180° to +180°; positive if the TAPS data lead) and the dots represent the phase at particular frequencies (1.95 and 3.89 cpd) that contain high variance determined from PSD. When coherence is high ($\gamma^2(f) > 0.78$), the phase is reliably estimated. A 24-h, 12.42-, and 6.21-h periodicities dominate the pattern of chlorophyll *a*. Peak of chlorophyll *a* led maximal flood tidal speed by 1.3 h and led maximal tidal speed by 1.9 h. A 12.42-h periodicity dominates particulate backscattering coefficients pattern, which led maximal tidal speed by 2.2 h.

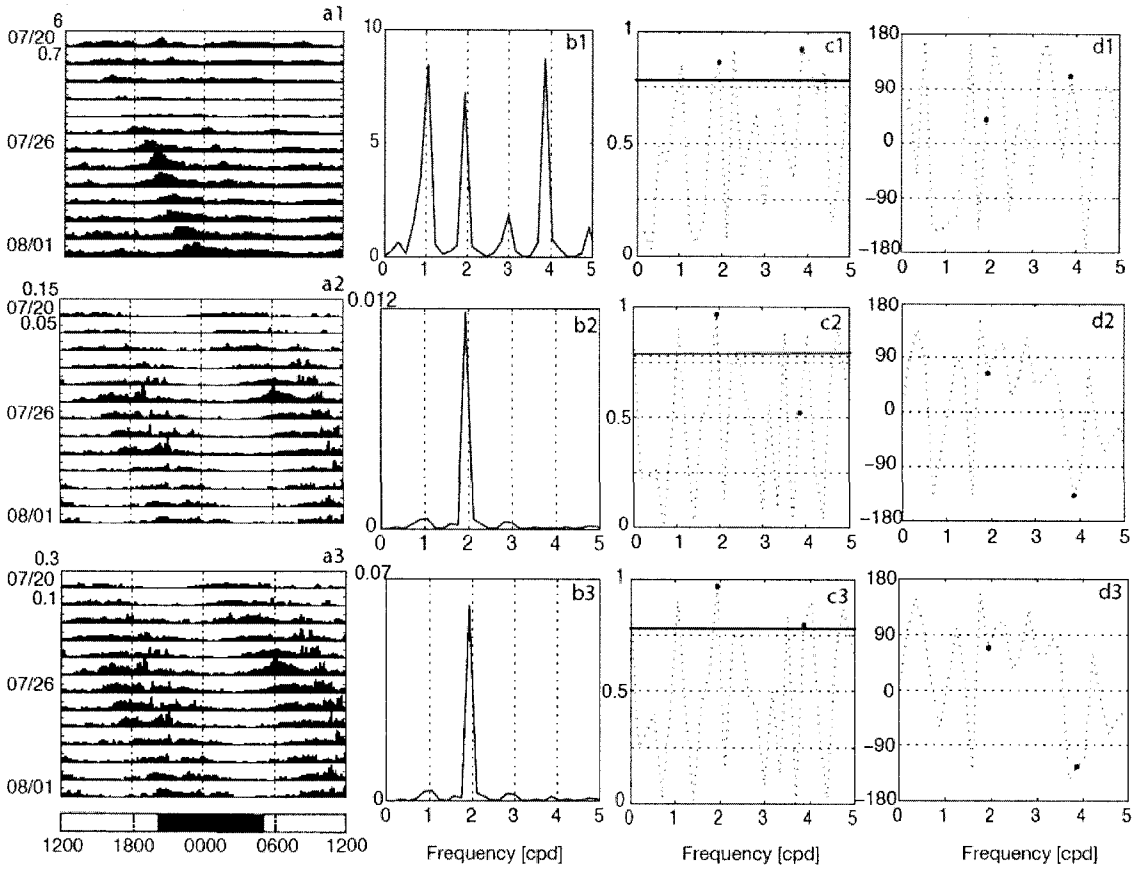
a1
6
07/20
0.7
07/26
08/01
b1
10
5
0
c1
1
0.5
0
d1
180
90
0
−90
−180
a2
0.15
07/20
0.05
07/26
08/01
b2
0.012
0
c2
d2
a3
0.3
07/20
0.1
07/26
08/01
b3
0.07
c3
d3
0 1 2 3 4 5
1200 1800 0000 0600 1200
Frequency [cpd]
Frequency [cpd]
Frequency [cpd]

Figure 3.12. Time series and spectral analysis of S_v at 265 kHz in 2006. (a) Representative echograms (265 kHz) over a 3-d period from 21 to 23 July 2006. Date tick marks correspond to midnight. Water depth varied with tidal phase, but the plot has been truncated uniformly at 10 mab. (b) Temporal fluctuations in the intensity of S_v plotted on a 24-h time scale at 7 (b1), 3 (b2), 1 (b3) and 0.25 mab (b4). Decibel levels are shown only for the first date (upper left corner of each panel). Note that the decibel levels are chosen to show the clear pattern, therefore, it is not consistent among figures. (c) PSD estimates [dB^2 Hz^{-1}] for S_v at 7 (c1), 3 (c2), 1 (c3) and 0.25 mab (c4). Diel periodicity is strongest closest to the bottom in phase with darkness. Elsewhere, tidal periodicities of 12.42- and 6.21-h shared dominance.

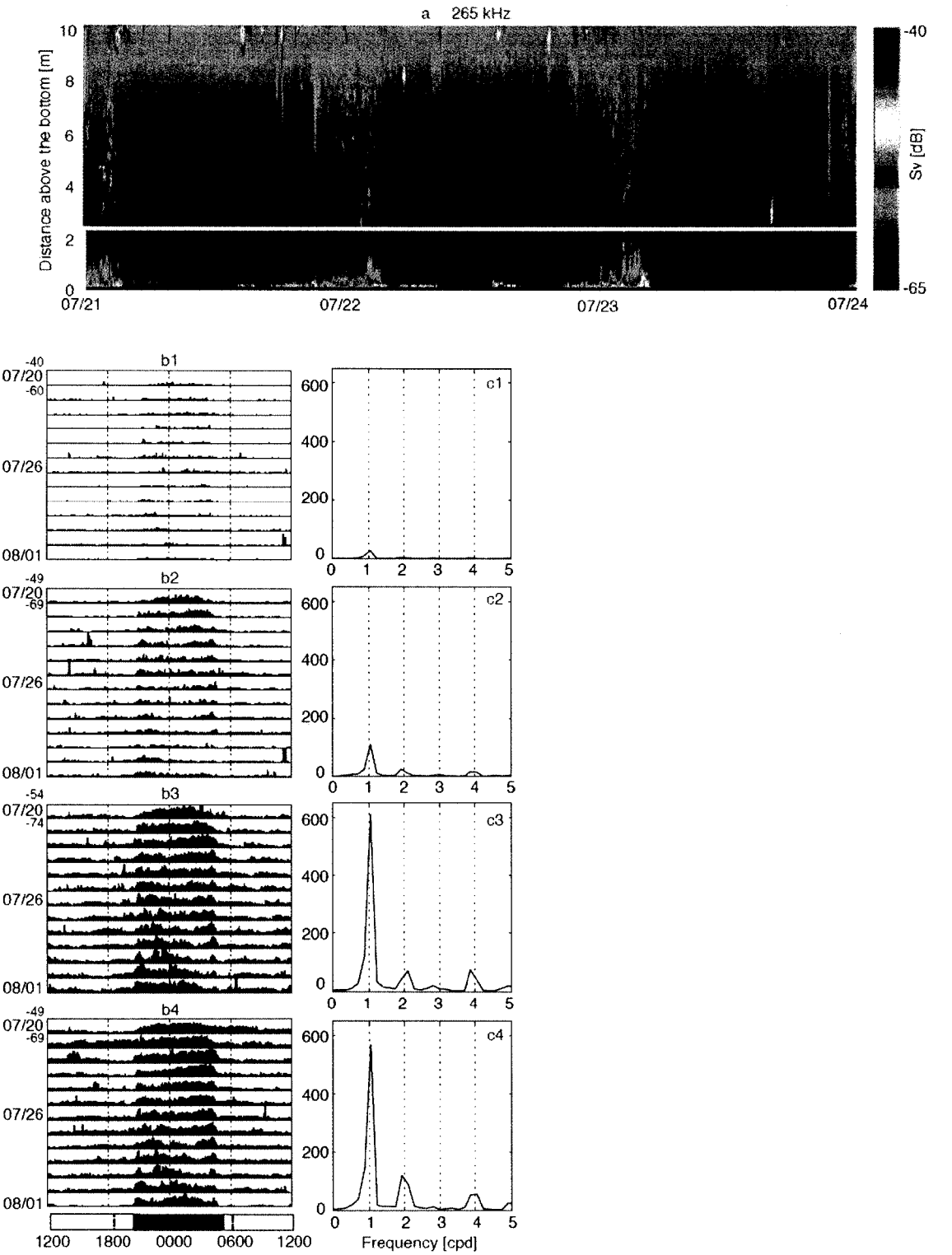
a 265 kHz
Distance above the bottom [m]
10
8
6
4
2
0
07/21
07/22
07/23
07/24
-40
-65
Sv [dB]
b1
b2
b3
b4
c1
c2
c3
c4
-40
-60
-49
-69
-54
-74
07/20
07/26
08/01
600
400
200
0
0 1 2 3 4 5
1200 1800 0000 0600 1200
Frequency [cpd]

Figure 3.13. Time series and spectral analysis of S_v at 420 kHz in 2006. (a) Representative echograms (420 kHz) over a 3-d period from 21 to 23 July 2006. Date tick marks correspond to midnight. Water depth varied with tidal phase, but the plot has been truncated uniformly at 10 mab. (b) Temporal fluctuations in the intensity of S_v plotted on a 24-h time scale as a waterfall plot at 7 (b1), 3 (b2), 1 (b3) an 0.25 mab (b4). Decibel levels are shown only for the first date (upper left corner of each panel). (c) PSD estimates [dB^2 Hz^{-1}] for S_v at 7 (c1), 3 (c2), 1 (c3) and 0.25 mab (c4). (d) Squared coherence, $\gamma^2(f)$, spectra at 7 (d1), 3 (d2), 1 (d3) and 0.25 mab (d4). Line indicates 95% confidence level. The broken line represents the value of $\gamma^2(f)$ (between 0 and 1) and the dots represent $\gamma^2(f)$ at particular frequencies (1.93 and 3.87 cpd) that contain high variance determined from PSD. (e) Phase spectra [degrees] at 7 (e1), 3 (e2), 1 (e3) and 0.25 mab (e4). The broken line represents estimated phase (-180° to +180°; positive if the TAPS data lead) and the dots represent the phase at particular frequencies (1.93 and 3.87 cpd) that contain high variance determined from PSD. When coherence is high ($\gamma^2(f) > 0.78$), the phase is reliably estimated. Near the bottom, diel periodicity was strongest and in phase with darkness, but throughout the water column, tidal periodicities shared spectral power.

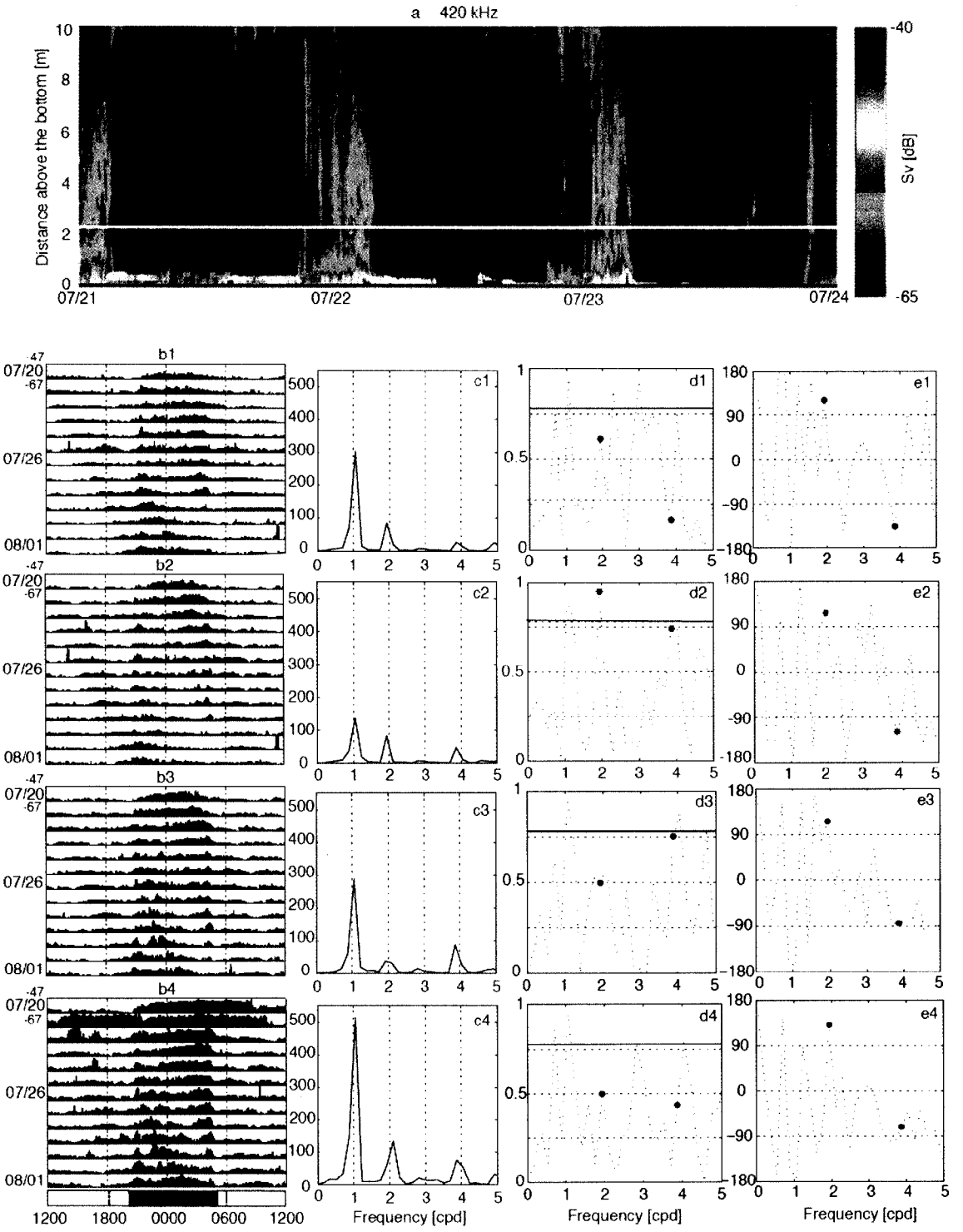
a 420 kHz
Distance above the bottom [m]
10
8
6
4
2
0
07/21
07/22
07/23
07/24
-40
-65
Sv [dB]
b1
b2
b3
b4
c1
c2
c3
c4
d1
d2
d3
d4
e1
e2
e3
e4
-47
-67
07/20
07/26
08/01
1200
1800
0000
0600
1200
Frequency [cpd]
Frequency [cpd]
Frequency [cpd]

Figure 3.14. Time series and spectral analysis of S_v at 700 kHz in 2006. (a) Representative echograms (700 kHz) over a 3-d period from 21 to 23 July 2006. Date tick marks correspond to midnight. Water depth varied with tidal phase, but the plot has been truncated uniformly at 10 mab. (b) Temporal fluctuations in the intensity of S_v plotted on a 24-h time scale as a waterfall plot at 7 (b1), 3 (b2), 1 (b3) and 0.25 mab (b4). Decibel levels are shown only for the first date (upper left corner of each panel). (c) PSD estimates [dB^2 Hz^{-1}] for S_v at 7 (c1), 3 (c2), 1 (c3) and 0.25 mab (c4). (d) Squared coherence, $\gamma^2(f)$, spectra at 7 (d1), 3 (d2), 1 (d3) and 0.25 mab (d4). Line indicates 95% confidence level. The broken line represents the value of $\gamma^2(f)$ (between 0 and 1) and the dots represent $\gamma^2(f)$ at particular frequencies (1.93 and 3.87 cpd) that contain high variance determined from PSD. (e) Phase spectra [degrees] at 7 (e1), 3 (e2), 1 (e3) and 0.25 mab (e4). The broken line represents estimated phase (-180° to +180°; positive if the TAPS data lead) and the dots represent the phase at particular frequencies (1.93 and 3.87 cpd) that contain high variance determined from PSD. When coherence is high ($\gamma^2(f) > 0.78$), the phase is reliably estimated. Near the surface 12.42-h was the dominant periodicity in phase with low slack tides. Near the bottom, a diel periodicity was strongest and in phase with darkness.

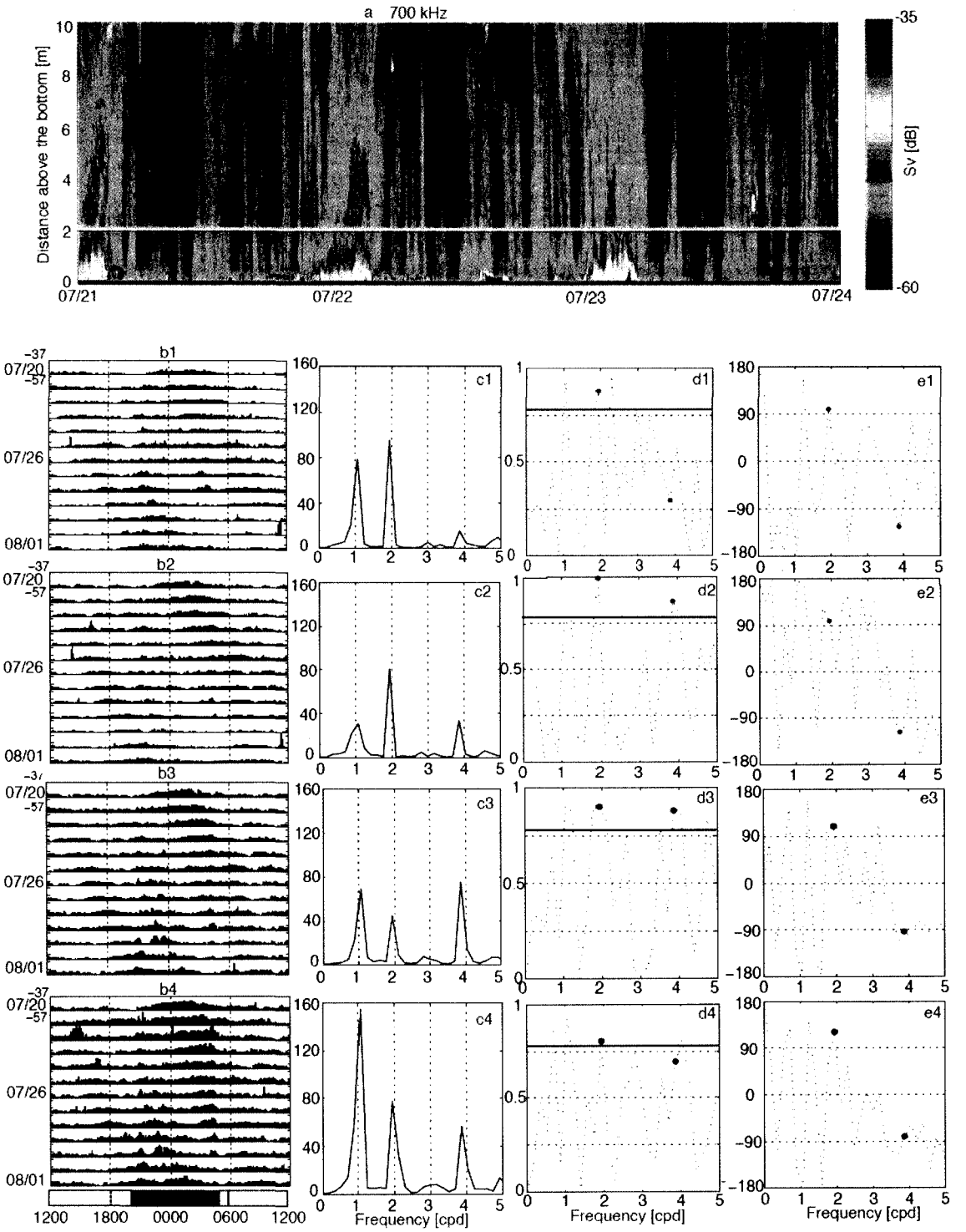
a 700 kHz
Distance above the bottom [m]
10
8
6
4
2
0
07/21
07/22
07/23
07/24
-35
-60
Sv [dB]
b1
b2
b3
b4
c1
c2
c3
c4
d1
d2
d3
d4
e1
e2
e3
e4
07/20
07/26
08/01
1200
1800
0000
0600
1200
Frequency [cpd]

Figure 3.15. Time series and spectral analysis of S_v at 1100 kHz in 2006. (a) Representative echograms (1100 kHz) over a 3-d period from 21 to 23 July 2006. Date tick marks correspond to midnight. Water depth varied with tidal phase, but the plot has been truncated uniformly at 10 mab. (b) Temporal fluctuations in the intensity of S_v plotted on a 24-h time scale at 7 (b1), 3 (b2), 1 (b3) and 0.25 mab (b4). Decibel levels are shown only for the first date (upper left corner of each panel). Note that the decibel levels are chosen to show the clear pattern, therefore, it is not consistent throughout the figures. (c) PSD estimates [dB^2 Hz^{-1}] for S_v at 7 (c1), 3 (c2), 1 (c3) and 0.25 mab (c4). (d) Squared coherence, $\gamma^2(f)$, spectra at 7 (d1), 3 (d2), 1 (d3) and 0.25 mab (d4). Line indicates 95% confidence level. The broken line represents the value of $\gamma^2(f)$ (between 0 and 1) and the dots represent $\gamma^2(f)$ at particular frequencies (1.93 and 3.87 cpd) that contain high variance determined from PSD. (e) Phase spectra [degrees] at 7 (e1), 3 (e2), 1 (e3) and 0.25 mab (e4). The broken line represents estimated phase (-180° to +180°; positive if the TAPS data lead) and the dots represent the phase at particular frequencies (1.93 and 3.87 cpd) that contain high variance determined from PSD. When coherence is high ($\gamma^2(f) > 0.78$), the phase is reliably estimated. Near the surface 12.42-h was the dominant periodicity, coincident with low slack tides; at other depths, 6.21-h periodicities shared dominance, lagging maximal current speeds by ~ 1.5 h.

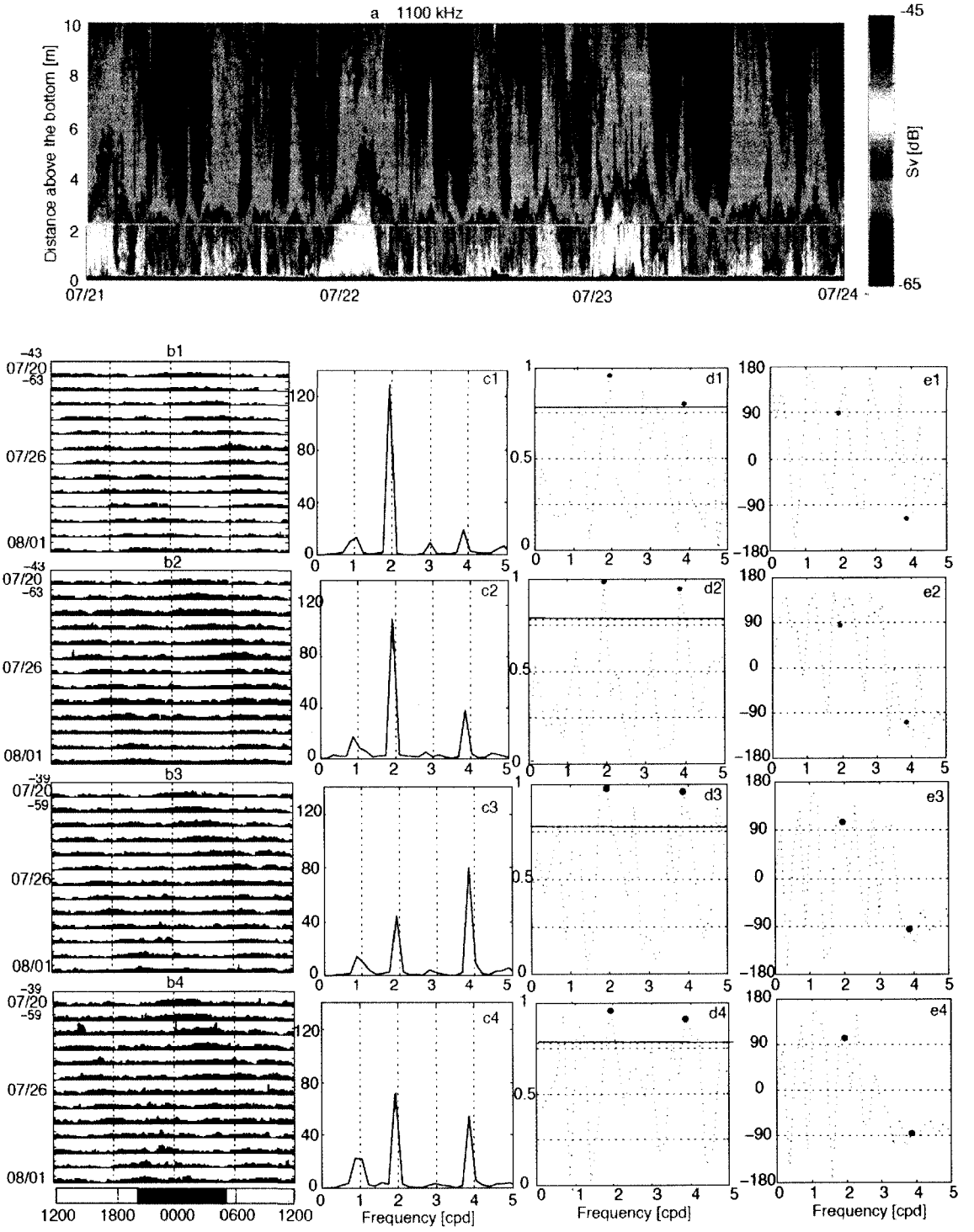
a 1100 kHz
Distance above the bottom [m]
10
8
6
4
2
0
07/21
07/22
07/23
07/24
-45
-65
Sv [dB]
b1
b2
b3
b4
-43
-63
-39
-59
07/20
07/26
08/01
c1
c2
c3
c4
d1
d2
d3
d4
e1
e2
e3
e4
Frequency [cpd]
1200
1800
0000
0600
1200

Figure 3.16. Time series and spectral analysis of S_v at 1850 kHz in 2006. (a) Representative echograms (1850 kHz) over a 3-d period from 21 to 23 July 2006. Date tick marks correspond to midnight. Water depth varied with tidal phase, but the plot has been truncated uniformly at 6 mab due to the range limitation at this frequency. (b) Temporal fluctuations in the intensity of S_v plotted on a 24-h time scale at 3 (b1), 1 (b2) an 0.25 mab (b3). Decibel levels are shown only for the first date (upper left corner of each panel). (c) PSD estimates [$dB^2\ Hz^{-1}$] for S_v at 3 (c1), 1 (c2) and 0.25 mab (c3). (d) Squared coherence, $\gamma^2(f)$, spectra at 3 (d1), 1 (d2) and 0.25 mab (d3). Line indicates 95% confidence level. The broken line represents the value of $\gamma^2(f)$ (between 0 and 1) and the dots represent $\gamma^2(f)$ at particular frequencies (1.93 and 3.87 cpd) that contain high variance determined from PSD. (e) Phase spectra [degrees] at 3 (e1), 1 (e2) and 0.25 mab (e3). The broken line represents estimated phase (-180° to +180°; positive if the TAPS data lead) and the dots represent the phase at particular frequencies (1.93 and 3.87 cpd) that contain high variance determined from PSD. When coherence is high ($\gamma^2(f) >$ 0.78), phase is reliably estimated. Periodicities of 12.42-h dominated, in phase with close to low slack tides, but 6.21-h periodicities also played a role.

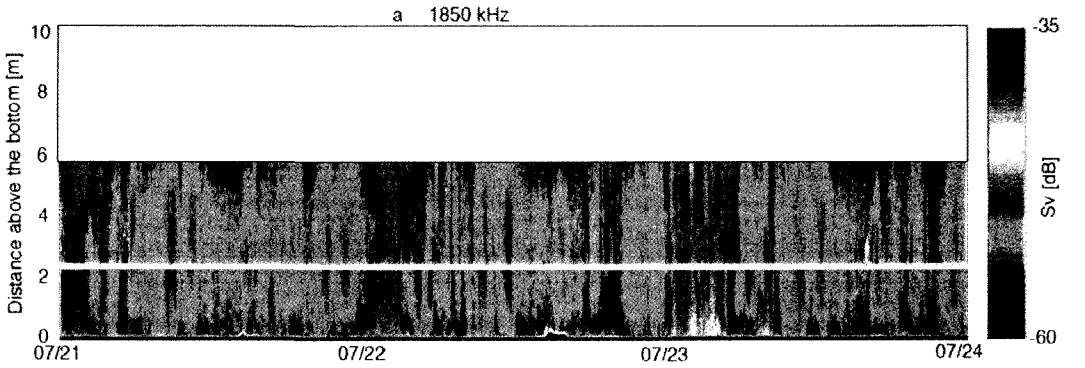
a 1850 kHz
Distance above the bottom [m]
10
8
6
4
2
0
07/21
07/22
07/23
07/24
-35
-60
Sv [dB]

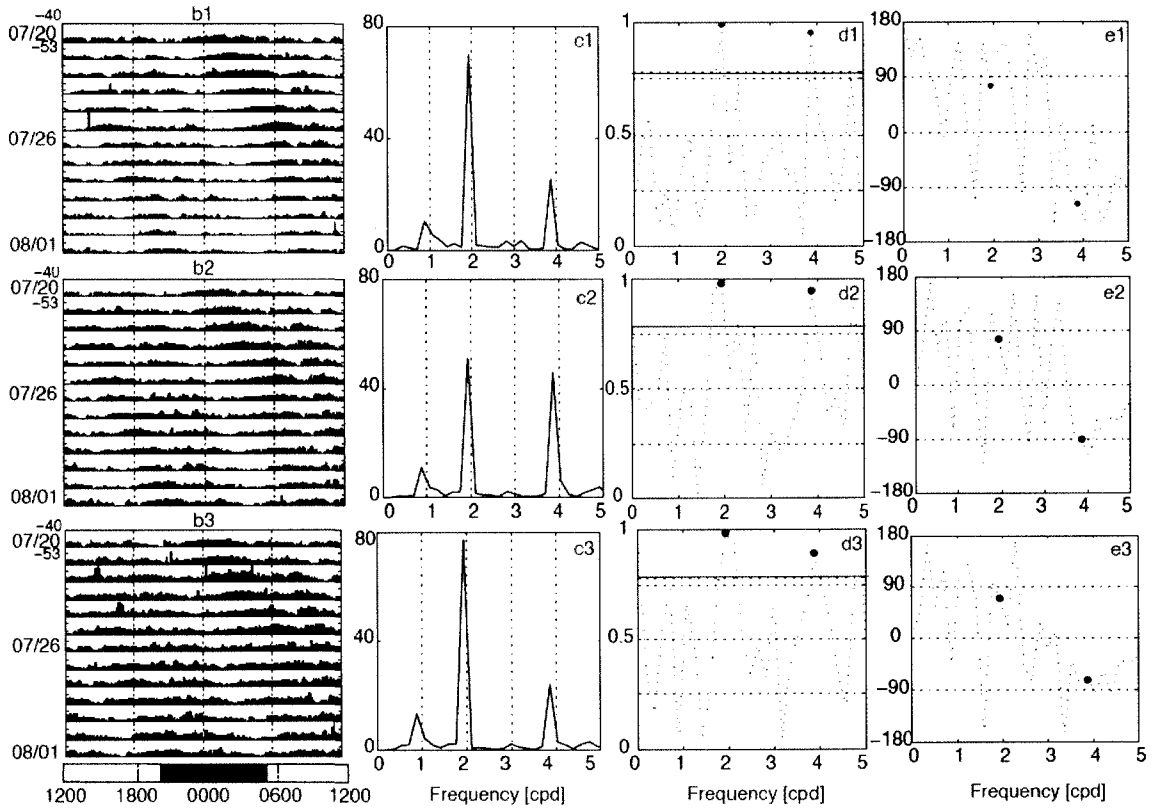
b1
b2
b3
-40
-53
07/20
07/26
08/01
1200
1800
0000
0600
1200
c1
c2
c3
d1
d2
d3
e1
e2
e3
Frequency [cpd]
Frequency [cpd]
Frequency [cpd]

Figure 3.17. Time series and spectral analysis of S_v at 3000 kHz in 2006. (a) Representative echograms (3000 kHz) over a 3-d period from 21 to 23 July 2006. Date tick marks correspond to midnight. Water depth varied with tidal phase, but the plot has been truncated uniformly at 4 mab due to the range limitation at this frequency. (b) Temporal fluctuations in the intensity of S_v plotted on a 24-h time scale at 3 (b1), 1 (b2) an 0.25 mab (b3). Decibel levels are shown only for the first date (upper left corner of each panel). (c) PSD estimates [$dB^2\ Hz^{-1}$] for S_v at 3 (c1), 1 (c2) and 0.25 mab (c3). (d) Squared coherence, $\gamma^2(f)$, spectra at 3 (d1), 1 (d2) and 0.25 mab (d3). Line indicates 95% confidence level. The broken line represents the value of $\gamma^2(f)$ (between 0 and 1) and the dots represent $\gamma^2(f)$ at particular frequencies (1.93 and 3.87 cpd) that contain high variance determined from PSD. (e) Phase spectra [degrees] at 3 (e1), 1 (e2) and 0.25 mab (e3). The broken line represents estimated phase (-180° to +180°; positive if the TAPS data lead) and the dots represent the phase at particular frequencies (1.93 and 3.87 cpd) that contain high variance determined from PSD. When coherence is high ($\gamma^2(f) >$ 0.78), the phase is reliably estimated. Periodicities of 12.42-h dominated at 3 mab, but 6.21-h periodicities were important at both 1 and 0.25 mab. Phase differences decreased toward the bottom at both periodicities.

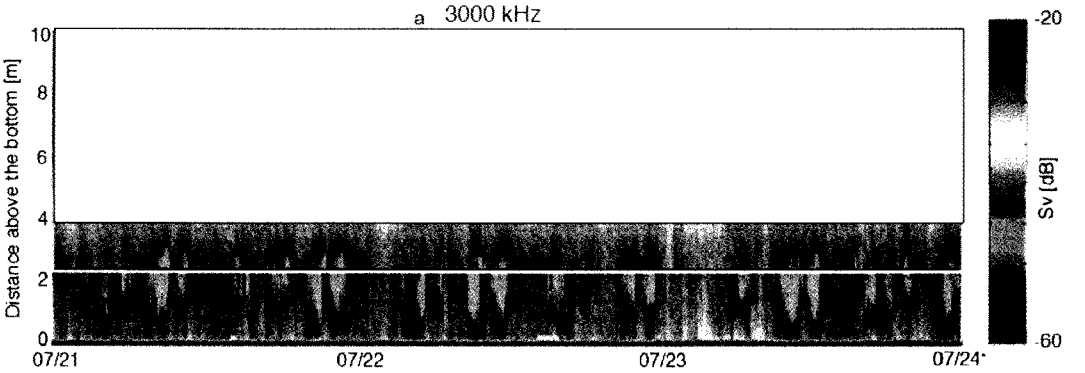
a 3000 kHz
Distance above the bottom [m]
10
8
6
4
2
0
07/21
07/22
07/23
07/24
-20
-60
Sv [dB]

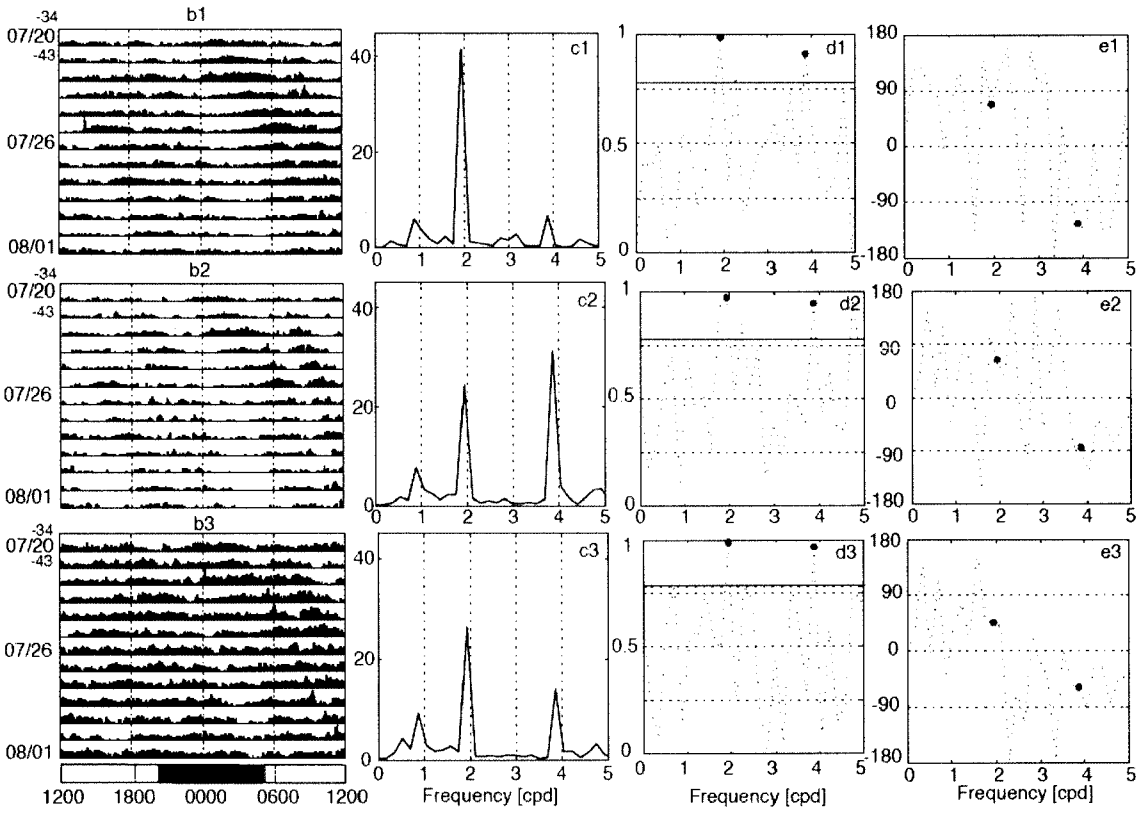
b1
b2
b3
-34
-43
07/20
07/26
08/01
1200
1800
0000
0600
1200
c1
c2
c3
d1
d2
d3
e1
e2
e3
Frequency [cpd]
Frequency [cpd]
Frequency [cpd]

Table 3.2. Summary of cross-spectral analyses between S_v, chlorophyll *a*, particulate backscattering coefficients at 470 nm (bbp470), and at 700 nm (bbp700), and tidal current speeds during field observations in 2006. Statistically significant squared coherences ($\gamma^2(f) > 0.78$) are summarized. A positive value of $\phi(f)$ implies the variation of data in TAPS or ECO-BB2F data to lead the variations of ADCP data.

	Distance	M_2 cycle (12.42 h)		$M_2/2$ cycle (6.21 h)	
	[mab]	$\gamma^2(f)$	$\phi(f)$	$\gamma^2(f)$	$\phi(f)$
265 kHz	7	-	-	-	-
420 kHz	7	-	-	-	-
700 kHz	7	0.88	98° (3.4 h)	-	-
1100 kHz	7	0.96	89° (3.1 h)	0.80	-118° (-2.0 h)
265 kHz	3	-	-	-	-
420 kHz	3	0.95	117° (4.0 h)	-	-
700 kHz	3	1.00	99° (3.4 h)	0.87	-118° (-2.0 h)
1100 kHz	3	0.99	85° (2.9 h)	0.95	-109° (-1.9 h)
1850 kHz	3	0.99	76° (2.6 h)	0.96	-117° (-2.0 h)
3000 kHz	3	0.99	68° (2.3 h)	0.91	-125° (-2.2 h)
265 kHz	1	-	-	-	-
420 kHz	1	-	-	-	-
700 kHz	1	0.90	110° (3.8 h)	0.88	-93° (-1.6 h)
1100 kHz	1	0.98	106° (3.7 h)	0.96	-96° (-1.7 h)
1850 kHz	1	0.98	76° (2.6 h)	0.95	-91° (-1.6 h)
3000 kHz	1	0.97	64° (2.2 h)	0.95	-85° (-1.5 h)
265 kHz	0.25	-	-	-	-
420 kHz	0.25	-	-	-	-
700 kHz	0.25	0.80	121° (4.2 h)	-	-
1100 kHz	0.25	0.96	103° (3.6 h)	0.91	-85° (-1.5 h)
1850 kHz	0.25	0.98	71° (2.5 h)	0.89	-73° (-1.3 h)
3000 kHz	0.25	0.99	47° (1.6 h)	0.97	-58° (-1.0 h)
chlorophyll *a*	4	0.86	39° (1.3 h)	0.92	110° (1.9 h)
bbp470	4	0.97	65° (2.2 h)	-	-
bbp700	4	0.97	65° (2.2 h)	-	-

Chapter 4

DISCUSSION

4.1. Mysid emergence

Strongest emergence of mysid was observed during the summer season, in which mysid showed a diel pattern as detected at 265-420 kHz throughout the water column. During this period, the onset of emergence corresponded to the onset of darkness. Toward the end of the emergence season, the diel cycle became weaker, and the dominant cycle for emergence shifted to the 12.42-h tidal periodicity, with different phasing near the surface and the bottom. Mysids emerging close to low slack tides moved rapidly to the water column near the surface. Close to flood tides, mysids also emerged but did not rise very high off the bottom. The shift of nocturnal to tidally oriented emergence can be explained by reduced phytoplankton concentration in the water column and termination of energetically expensive reproduction at the end of emergence season.

Nocturnal emergence of epibenthic animals has been reported by many workers (e.g., Kringel et al. 2003; Abello et al. 2005). Although *N. americana* is omnivorous and in our shallow-water setting, hyperbenthic animals have food sources available to them even during the daylight in the form of organic-matter-covered sediments, detritus, benthic diatoms, and meiofauna, feeding seems likely to be the ultimate driving force of nocturnal emergence. Because the quality of organic-matter-covered sediments or detritus is relatively low for the energy-intensive activities of egg production, migration in pursuit of richer food sources in the water column could provide metabolic advantage, particularly when benthic diatoms became scarce during mid summer (Abello et al.

2005). Feeding in the water column during the night is supported by the stomach content analysis of *Mysis mixta*, showing greater intake of zooplankton during the night and detritus during the day (Rudstam et al. 1989). Predator avoidance is also a possible driving force of the nocturnal emergence. Since mysids are major food sources for juveniles of bottom-dwelling fishes, mysids remain quiescent on or in bottom sediments during the day. The time-series analysis presented here, however, can only detect these cycles that are consistently observed throughout the observation period. Response to predator presence or other sporadic but potentially significant events can only weaken cycles and therefore cannot be detected as spectral analysis. Stress cause by the low oxygen concentrations near the bottom during the night is less likely the reason for nocturnal emergence in our study site. Observations conducted for a 4-d period in mid July 2002 showed no evidence of stressfully low oxygen concentration at the seabed in our study site (Vopel and Thistle, unpublished).

Tidally oriented emergence behaviors have been reported for many different types of zooplankton including fish larvae, copepods and mysids in the field, but sampling resolution of most previous studies was too low to resolve the exact timing of emergence relative to tidal currents (e.g., Wooldridge and Erasmus 1980; Palmer and Brandt 1981; Kimmerer et al. 1998). At the end of the emergence season when phytoplankton became scarce in the water column, the emergence pattern coincident with low slack tides can be explained by maximization of feeding on phytoplankton. Mysids were observed near the surface when chlorophyll *a* concentration reaches its daily maximum due to advection from upstream in the estuary. Also, by emerging during low slack tides, animals can minimize the risk of being flushed out of the estuary, because

during the subsequent flood tide, they would be carried upstream by tidal currents. Our observation suggests that *N. americana* uses flood tides for horizontal transport near the bottom of the Damariscotta River estuary. The tidally phased emergence has previously been observed in our study site by Taylor et al. (2005), but emergence trap collections could not confirm the movement of animals with tides near the bottom. This is due to the design of emergence traps, which only allows us to capture and quantify organisms moving vertically > 1 m from the bottom, but not the ones moving horizontally. In 2005, we often observed numerous *N. americana* deposited on the outside of the netting of the emergence trap, which supports the horizontal transport mechanism. Similar utilization of flood tides and avoidance of ebb tides near the bottom has been observed in *Rhopalophthalamus terranatalis* in South African estuaries (Wooldridge and Erasmus 1980), and *N. americana* in Narragansett Bay, Rhode Island (Herman 1963). The timing of emergence resolved in this study suggests that some animals avoid the fastest current speed, indicting there might be a threshold speed to which animals react.

4.2. Emergence of smaller animals

In fall 2005, the smaller animals detectable at 1100–3000 kHz, which were likely dominated by copepods, were mostly regulated by tidal period components of 12.42 and 6.21 h. The 12.42-h component dominated near the surface, while the 6.21-h component became more important toward the bottom. The phasing with tidal components of 12.42- and 6.21-h periods varies depending on TAPS frequency. Higher S_v corresponds to close to the low slack tides, indicating the smaller organisms emerged and filled the water column. Close to the bottom (3 mab), higher S_v occurs 1.5-1.8 h after

the maximal tidal speed, suggesting animals avoided the fastest velocities and did not emerge high off the bottom. In summer 2006, however, 12.42-h periodicity dominated throughout the water column (7, 3, 0.25 mab), except at 1 mab. High S_v occurs 1.6-3.6 h before the maximal flood-tide, decreasing phase difference with increasing TAPS frequency. For 6.21-h periodicity, high S_v occurs 1.0-2.2 h after the maximal tidal speed. The emergence periodicity of 6.21 h has only been reported in copepods by Gagnon and Lacroix (1981). Since smaller organisms can be expected to migrate shorter distances from the bottom, water-column integrated sampling by plankton nets or traps may have too little vertical resolution to resolve the 6.21-h period. Particulate backscattering data in 2005 clearly shows that suspended particles from the bottom increase at maximal flood tide, whose current velocity is stronger than ebb tide. Since the phasing of S_v at 1100-3000 kHz with tidal components is clearly different from that of particulate backscattering, the observed S_v patterns are due to the biological activities rather than resuspension of sediment into the water column via tidal currents. Differential utilization of tidal currents and timing of emergence among species (Wooldrige and Erasmus 1980; Saigusa 2001) and different sizes (Hays et al. 2001) of organisms has been reported. There are likely multiple species contributing to the acoustic data, and the biological samples of smaller organisms are required to distinguish among species in order to obtain further understanding of emergence mechanism of smaller animals.

4.3. Perception of timing by mysids

Zooplankton have the capacity to control their vertical positions in response to light gradients and probably, for species adapted to estuarine environments, in response to

tidal rhythms, thereby interacting with two-layer circulation systems in more complicated and precise ways than nonliving particles (Runge and Simard 1990). The phototactic responses of *N. americana* have been examined by Herman (1962). In general, mysids are attracted to weak sources of light, but avoid bright light which often inhibits swimming activity. A regular and important aspect of twilight under water is its spectral shift in wavelength of maximal transmission from shorter, blue, to longer, blue-green, wavelengths (Forward 1988). Zooplankton spectral sensitivity has been shown to match that of wavelengths prevalent during twilight, 475 to 525 nm (Forward 1988) in coastal and estuarine waters. *N. americana* has reported *in vitro* peak sensitivity at 515 nm (Herman 1962).

Low $\gamma^2(f)$ at 12.42-h periodicity of cross-spectral analysis between S_v and tidal currents both collected at 7 mab (not shown) compared to high $\gamma^2(f)$ of cross-spectral analysis between S_v at 7 mab and tidal currents at 3 mab strongly indicate that mysids are responding to the near-bottom current speed. Statocysts, which are gravity receptors, are present in the uropods of mysids (Mauchline 1980). Although Rice (1961, 1964) found that the effects of gravity dominated those of light in the orientation process and increase in hydrostatic pressure caused the mysids to move upwards in the water column, it does not explain the upward behavior at low slack tides in this study. The movements of epibenthic organisms associated with the tidal cycle could more likely be cued by tidal variations in salinity, temperature, dissolved organics, turbidity or other water quality parameters.

4.4 Conclusion and implications of the study

Fundamental issues of benthic-pelagic coupling are how many organisms of what species and size classes transit both habitats and how they allocate time to subsets of those habitats. It is virtually impossible to gain high resolution of these issues through classical net sampling in a dynamic nearshore or estuarine setting. Biological interactions require encounter, and rates of encounter depend upon local organism abundances, velocities and perception distances. Although TAPS does not resolve individuals it does allow highly spatially resolved estimation of abundances and net group velocities (e.g., Kringel 2003).

Turbulence caused by migration events can enhance nutrient mixing (Kunze et al. 2006) and this study suggests that the degrees of mixing in ecosystems may vary with depth and season, depending on species composition and ontogenetic stage. Resolution of temporal and spatial sampling frequency is also critical to understand mechanisms and components of emergence. For example, the phenomenon widely known as midnight sinking has been reported in mysid species (Herman 1963; Macquart-Moulin and Ribera Maycas 1995; Kringel et al. 2003 and Taylor et al. 2005 reviewed by Jumars 2007). Mysids tend to be less abundant near the surface near midnight than just after sunset or just before dawn. However, the two-week field observation during the strong mysid emergence period in 2006 revealed that apparent midnight sinking in this setting was due to the combination of 24- and 12.42-h rhythms overlapping each other at night (e.g., 28-29 July 2006 shown in Figs. 3.12-3.13 b1-b2). This overlap also explains the dawn ascent noted by Herman (1963). Although tidal modulation is unlikely to explain all prior observations of midnight sinking, including the one conducted at a tidally weak

study site by Macquart-Moulin and Ribera Maycas (1995), this study clearly shows the importance of high sampling resolution especially at tidally regulated ecosystems.

Having six frequencies in acoustic observations, estimates of biovolumne of different size categories could be obtained by through a DWBA (distorted-wave, Born approximation) model for an elongate organism (McGehee et al. 1998) and a truncated sphere model for copepods. This was not possible in the present study because of unexpected problems in calibration offsets between the two TAPS. Sampling and identification of smaller organisms could help to separate signals caused by different species and to isolate factors driving emergence behaviors of each species. The spectral analysis presented here can only recognize the cycles consistently observed throughout the observation period, but patterns such as the high S_v observed on 20-21 July 2006 near the bottom even during the day require further research on sporadic events.

This study suggests from the results at 265 and 420 kHz that nocturnal mysid emergence during the summer is driven by requirement of high-quality food for reproduction. The shift in dominant mysid periodicity to an M_2 cycle toward the end of the emergence season, with differential use of tidal currents across depths, can be related to the availability of food sources in the water column and ontogenic changes in mysid behavior. Depth and seasonal dependence of multiple emergence events by epibenthic animals will certainly affect the degrees and nature of benthic-pelagic coupling.

REFERENCES

Abello, H.U.,Shellito, S.M., Taylor L.H., Jumars, P.A. 2005. Light-cued emergence and re-entry events in a strongly tidal estuary. Estuaries 28: 487-499.

Armonies, W. 1988. Active emergence of meiofauna from intertidal sediment. Marine Ecology Progress Series 43: 151-159.

Bell, S.S., Hicks, G.R.F., Walters, K. 1988. Active swimming in meiobenthic copepods of seagrass beds: species patterns and role in reproductive behavior. Marine Biology 98: 351-358.

David, V., Sautour, B., Galois, R., Chardy, P. 2006. The paradox [of] high zooplankton biomass-low vegetal particulated organic matter in high turbidity zones: What way for energy transfer? Journal of Experimental Marine Biology and Ecology 333:202- 218.

De Robertis, A., Jaffe J. S., Ohman M.D. 2000. Size-dependent visual predation risk and the timing of vertical migration in zooplankton. Limnology and Oceanography 45: 1838-1844.

De Witt, T.H. 1987. Microhabitat selection and colonization rates of a benthic amphiod. Marine Ecology Progress Series 36: 237-250.

Dodson, J.J., Dauvin, J.G., Ingram, R.G., D'Anglejan, B. 1989. Abundance of larval rainbow smelt (*Osmerus mordax*) in relation to the maximum turbidity zone and associated macroplanktonic fauna of the middle St. Lawrence Estuary. Estuaries 12: 66-81.

Emery, W.J., Thomson, R.E. 2001. Data analysis methods in physical oceanography. Elsevier. Second and revised edition. Amsterdam, The Netherlands. 638pp.

Fleeger J.W., Chandler, G.T., Fitzhugh, G.R., Phillips, F.E. 1984. Effects of tidal currents on meiofauna densities on vegetates salt marsh sediments. Marine Ecology Progress Series 19: 49-53.

Forward, R.B. 1988. Diel vertical migration: Zooplankton photobiology and behavior. Oceanography and Marine Biology Annual Review 26: 361-393.

Forward, R.B., Tankersley, R.A. 2001. Selective tidal-stream tranport of marine animals. 39: 305-353.

Friedland, K.D., Bejda, G.C., Sudholme, A.L. 1988. Interannual variation in diet and condition in juvenile bluefish during estuary residency. Transactions of the American Fisheries Society 117: 474-479.

Gagnon, M., Lacroix, G. 1981. Zooplankton sample variability in a tidal estuary: An interpretative model. Limnology and Oceanography 26: 401-413.

Grabe, S.A. 1980. Food of age 1 and 2 Atlantic tomcod, *Microgadus tomcod*, from Haverstraw Bay, Hudson Bay, Hudson River, New York. Fishery Bulletin 77: 1003-1006.

Hacunda, J.S. 1981. Trophic relationships among demersal fishes in a coastal area of the Gulf of Maine. Fishery Bulletin 79: 775-788.

Hanson, J.M., Chouinard, G.A. 2002. Diet of Atlantic cod in the southern Gulf of St Lawrence as an index of ecosystem change, 1959-2000. Journal of Fisheries Biology 60: 902-922.

Hays, G.C., Kennedy H., Frost B.W. 2001. Individual variability in diel vertical migration of a marine copepod: Why some individuals remain at depth when others migrate. Limnology and Oceanography 46: 2050-2054.

Hays, G.C. 2003. A review of the adaptive significance and ecosystem consequences of zooplankton diel vertical migrations. Hydribiologia 503: 163-170.

Herman, S. S. 1962. Spectral sensitivity and phototaxis in the opossum shrimp, *Neomysis americana* Smith. Biological Bulletin 123: 562-570.

Herman, S. S. 1963. Vertical migration of the opossum shrimp, *Neomysis americana* Smith. Limnology and Oceanography 8: 228-238.

Holliday, D.V., Pieper, R.E. 1980. Volume scattering strengths and zooplankton distributions at acoustic frequencies between 0.5 and 3 MHz. The Journal of the Acoustical Society of America 67: 135-146.

Holliday, D.V., Pieper, R.E. 1995. Bioacoustical oceanography at high frequencies. ICES Journal of Marine Science. 52: 279-296.

Jumars, P.A. 2007. Habitat coupling by mid-latitude, subtidal, marine mysids: important subsidized omnivores. Oceanography and Marine Biology: An Annual Review 45: *in press.*

Kimmerer, W.J., Burau, J.R., Bennett, W.A. 1998. Tidally oriented vertical migration and position maintenance of zooplankton in a temperate estuary. Limnology and Oceanography 43: 1697-1709.

Kringel, K., Jumars, P.A., Holliday, D.V. 2003. A shallow scattering layer: High-resolution acoustic analysis of nocturnal vertical migration from the seabed. Limnology and Oceanography 48: 1223-1234.

Kunze, E., Dower, J.F., Beveridge, I., Dewey, R., Bartlett, K. 2006. Observations of biologically generated turbulence in a coastal inlet. Science 313:1768-1770.

Lankford, T.E., Targett, T.E. 1997. Selective predation by juvenile weakfish: post-consumptive constraints on energy maximization and growth. *Ecology* 78: 1049-1061.

Lee, W.Y., McAlice, B.J. 1979. Seasonal succession and breeding cycles of three species of *Acartia* (Copepoda: Calanoida) in a Maine estuary. Estuaries 2: 228-235.

Lee, W.Y. 1978.The cyclopoid copepods, *Hemicycops adhaerens* and *Saphirela* sp., in the Damariscotta River estuary, Maine, with a note to their possible relationship. Estuaries 1: 200-202.

Link, J.S., Garrison, L.P. 2002. Trophic ecology of Atlantic cod *Gadus morhua* on the northeast U.S. continental shelf. Marine Ecology Progress Series 27: 109-123.

Macquart-Moulin, C., Ribera Maycas, E. 1995. Inshore and offshore diel migrations in European benthopelagic mysids, genera *Gastrosaccus, Anchialina* and *Haplostylus* (Crustacea, Mysidacea). *Journal of Plankton Research* **17,** 531-555.

Marcus, N.H., Boero, F. 1998. Minireview: the importance of benthic-pelagic coupling and the forgotten role of life cycles in coastal aquatic systems. Limnology and Oceanography 43: 763-768.

Mauchline, J. 1980. The biology of mysids and euphausiids. *Advances in Marine Biology* 18: 1-681.

Mayer, L.M., Townsend, D.W., Pettigrew, N.R., Loder, T.C., Wong, M.W., Kistner-Morris, D., Laursen, A.K., Schoudel, A.D., Conairis, C., Brown, J., Newell. C. 1996. The Kennebec, Sheepscot and Damariscotta River estuaries: Seasonal oceanographic data. University of Maine, Department of Oceanography Technical Report No. 1: 1-119. Walpole, Maine.

McAlice, B.J. 1993. Environmental characteristics of the Damariscotta River estuary, Maine. Darling Marine Center, Special Publication No. 1: 1-119. Walpole, Maine.

McGehee, D.E., O'Driscoll, R.L., Martin-Traykovski, L.V. 1998. Effects of orientation on acoustic scattering from Antarctic krill at 120 kHz. Deep-Sea Research II 45: 1273-1294.

Palmer, J.D. 1967. Daily and tidal components in the persistent rhythmic activity of the crab, *Sesarma*. Nature 215: 64-66.

Palmer, M.A., Brandt R.R. 1981. Tidal variation in sediment densities of marine benthic copepods. Mar. Ecol. Prog. Ser. 4: 207-212.

Pezzack, D.S., Corey, S. 1979. The life history and distribution of *Neomysis americana* (Smith) (Crustacea, Mysidacea) in Passamaquoddy Bay. Canadian Journal of Zoology 57: 785–793.

Pinot, J.M., Jansa, J. 2001. Time variability of acoustic backscatter from zooplankton in the Ibiza Channel (western Mediterranean). Deep-Sea Research I 48: 1651-1670.

Rachin, J.W., Warkentine, B.E. 1988. Feeding preference of sympatric hake from the inner New York Bight. Annals of the New York Academy of Sciences 529: 157-159.

Rice, A.L. 1961. The response of certain mysids to changes in hydrostatic pressure. Journal of Experimental Biology 18: 659-671.

Rice, A.L. 1964. Observations on the effects of changes of hydrostatic pressure on the behaviour of some marine animals. Journal of the Marine Biological Association of the United Kingdom 44: 163-175.

Roast, S.D., Widdows, J., Pope, N., Jones, M.B. 2004. Sediment-biota interactions: mysid feeding activity enhances water turbidity and sediment erodability. Marine Ecology Progress Series 281: 145-154.

Ross, S.W. 1989. Diet of the banded drum in North Carolina. Transactions of the American Fisheries Society 118: 680-686.

Rudstam, L.G., Danielsson, K., Hansson, S., Johansson, S. 1989. Diel vertical migration and feeding patterns of *Mysis mixta* (Crustacea, Mysidacea) in the Baltic Sea. Marine Biology 101: 43-52.

Runge, J.A., Simard, Y. 1990. Zooplankton of the St. Lawrence estuary: The imprint of physical processes on its composition and distribution. Coastal and Estuarine Studies 39: 296-320.

Saigusa, M. 2001. Daily rhythms of emergence of small invertebrates inhabiting shallow subtidal zones: A comparative investigation at four locations in Japan. Ecological Research 16: 1-28.

Sanders, R.W. 1987. Tintinnids and other microzooplankton – seasonal distributions and relationships to resources and hydrography in a Maine estuary. Journal of Plankton Research 9: 65-77.

Takahashi, K., Kawaguchi, K. 1997. Diel and tidal migrations of the sand-burrowing mysids, *Archaeomysis kokuboi*, *A. japonica* and *Iiella ohshimai*, in Otsuchi Bay, northeastern Japan. Marine Ecology Progress Series 148: 95-107.

Taylor, L.H., Shellito, S.M., Abello, H.U., Jumars, P.A. 2005. Tidally phased emergence events in a strongly tidal estuary. Estuaries 28: 500 – 509.

Teasdale, M., Vopel, K. Thistle, D. 2004. The timing of benthic copepod emergence. Limnology and Oceanography 49: 884-889.

Thistle, D. 2003. Harpacticoid copepod emergence at a shelf site in summer and winter: implications for hydrodynamic and mating hypotheses. Mar. Ecol. Prog. Ser. 248: 177-185.

Thompson, B.P. 2006. Temporal and spatial variability of phytoplankton biomass in the Damariscotta River estuary, Maine, USA. M.S. Thesis, Univ. of Maine, 89 pp.

Townsend, D.W. 1983. The relations between larval fishes and zooplankton in two inshore areas of the Gulf of Maine. Journal of Plankton Research 5: 145-171.

Vopel, K., Dehmlow, J., Johansson, M., Arlt, G. 1998. Effects of anoxia and sulphide on populations of *Cletocamptus confluens* (Copepoda, Harpacticoida). Marine Ecology Progress Series 175: 121-128.

Vopel, K., Arlt, D.G. 1996. Vertical distribution of *Cletocamptus confluens* (Copepoda, Harpacticoida) in relation to oxygen and sulphide microprofiles of a brackish water sulphuretum. Marine Ecology Progress Series 141: 129-137.

Walters, K., Bell, S.S. 1994. Significance of copepod emergence to benthic, pelagic, and phytal linkages in a subtidal seagrass bed. Marine Ecology Progress Series 108: 237-249.

Wiebe, P.H., Benfield, M.C. 2003. From the Hensen net toward four-dimensional biological oceanography. Progress in Oceanography 56: 7-136.

Wooldridge, T., Erasmus, T. 1980. Utilization of tidal currents by estuarine zooplankton. Estuarine and coastal marine science 11: 107-114.

BIOGRAPHY OF THE AUTHOR

Mei Sato was born in Boston, Massachusetts on February 20, 1982. She was raised in Sendai, Japan and graduated from the Miyagi First Women High School in 2000. She attended to the Tokyo University of Fisheries and graduated in 2004 with a Bachelor's degree in Science. She entered the Oceanography graduate program at The University of Maine in the summer of 2004.

Mei is a candidate for the Master of Science degree in Oceanography from The University of Maine in December, 2006.